Theses and Dissertations

Summer 2010

# Advancements of a servohydraulic human hip joint motion simulator for experimental investigation of hip joint impingement/dislocation

Nicholas James Stroud
*University of Iowa*

## Recommended Citation

ADVANCEMENTS OF A SERVOHYDRAULIC HUMAN HIP JOINT MOTION

SIMULATOR FOR EXPERIMENTAL INVESTIGATION OF HIP JOINT

IMPINGEMENT/DISLOCATION

by

Nicholas James Stroud

A thesis submitted in partial fulfillment
of the requirements for the Master of
Science degree in Biomedical Engineering
in the Graduate College of
The University of Iowa

July 2010

Thesis Supervisor:  Professor Thomas D. Brown

Graduate College
The University of Iowa
Iowa City, Iowa

CERTIFICATE OF APPROVAL

_____

MASTER'S THESIS

_____

This is to certify that the Master's thesis of

Nicholas James Stroud

has been approved by the Examining Committee
for the thesis requirement for the Master of Science
degree in Biomedical Engineering at the July 2010 graduation.

Thesis Committee: _____
                     Thomas D. Brown, Thesis Supervisor


                  _____
                     Nicole Grosland


                  _____
                     Tae-Hong Lim


                  _____
                     Douglas Pedersen

ACKNOWLEDGMENTS

I wish to thank my advisor, Dr. Thomas Brown for his continual support, and for his patience. Especially while proof-reading the various abstracts and thesis drafts over the last two years. Additional gratitude is warranted for providing me the incredible opportunity to work in the Orthopaedic Biomechanics Laboratory.

Thanks to Dr. James Rudert for always having the time to answer my questions, and provide valuable feedback. And to whom much of my experience and knowledge gained over the years is a direct result of.

Thanks to Dr. Yuki Tochigi for always making the time to answer questions about anatomy, and perform hours of specimen preparation. Without his skill, there would be no results section.

Thanks to Jacob Elkins, for his insight and support with the many technical problems, and for making the last two years of office life both enjoyable and educational.

Additional thanks to Julie Mock, for all of her assistance, Nicole Kunze, Lu Kang, and co-workers for their help and support. Financial support was provided by the Department of Veterans Affairs and by NIH AR053553.

TABLE OF CONTENTS

iii

# LIST OF TABLES

v

## LIST OF FIGURES

ix

# TABLE OF EQUATIONS

CHAPTER I: INTRODUCTION

## 1.1 Primary and Revision Total Hip Arthroplasty

From humble beginnings in the late 19th century, total hip arthroplasty (THA) has become one of the most cost-effective orthopaedic surgeries[1, 2] and has been praised as one of the greatest surgical procedures in 20th century healthcare.[3] THA provides long term relief from debilitating pain, re-establishes mobility, and improves the overall quality of life for the patient.[4, 5] Nearly 90% of THA patients feel that their expectations have been met in post-operative pain reduction.[6] Published success rates have been estimated to be between 90 – 95% at 10 years post operation,[7-9] with an 83% probability of survival at 20 years, establishing THA as a long-term solution for hip diseases such as osteoarthritis, rheumatoid arthritis, congenital hip disease (dysplasia), and fractures (femoral neck).

THA, however, does not eliminate pain and re-establish mobility for all patients. Various implant failure modalities have been attributed to the patient, surgeon, as well as implant components. Common failure modalities include joint instability, aseptic component loosing, and infection. Failure frequently results in revision surgery, and upwards of 11 to 18% of primary THA procedures require revision at some point.[10, 11] Revision surgery is significantly more costly,[12] and has much lower rates of survivorship. Costs attributed to greater hospital resource use, such as longer hospital stays and recovery time, additional pre-operative planning and operating time, anesthesia, various life support products, and increased post-operative physical therapy all contribute to an increase in cost over primary THAs.[13] In tandem with higher monetary cost, revisions have a significantly reduced long term survivorship. Increased intra-operative bone and soft-tissue damage, coupled with a higher incidence of post-operative complications such as instability, aseptic loosening, and infection contribute to reduced survivorship in revision THAs. After the first revision surgery, 10 year post-operative survivorship drops

to 72.1%. After the second revision surgery, 10 year post-operative survivorship is reduced even further, to 59.5%.[10] As an increase in life expectancy and a higher quality of life are expected for current pre-retirement generations, the limits of implant longevity and component robustness will certainly be tested. If the current trends are allowed to continue, rates of revision arthroplasty will increase,[114] furthering their socio-economic burden.

## 1.2 Total Hip Arthroplasty Failure

Among the most frequent causes of implant failure that lead to revision surgery, instability and dislocation (22.5% of all revisions) have recently been demonstrated to numerically exceed aseptic loosening (19.7% of all revisions) and infection (14.8% of all revisions).[15] Dislocation has a variety of potential contributing factors that can occur individually or in concert. These factors are related to the patient, surgeon, and implant. A patient's non-adherence to physical activity guidelines, and generally having a physically active disposition, can lead to a higher incidence of dislocation. The placement of the prosthesis, surgical approach, and frequency that the surgeon performs the surgery have also been demonstrated to contribute to long-term survivorship. In addition to patient- and surgeon-associated risk factors, implant parameters, such as the head-to-neck ratio, should also be added to the list.[16] In recent years, attention has been drawn to the study of dislocation, and a significant body of literature has been published with the intention of determining risk factors. There is little concensus in the surgical community over which surgical approach is best in reducing the rates of dislocation.[17]

## 1.3 Risk Factors for Total Hip Dislocation

Various approaches have been described in the last half century, but the most commonly practiced methods are the anterolateral (described by von Spregel in 1878, and Bardenheuer in 1907) and posterior[18] approaches. In the anterolateral approach, access to the joint is through the tensor fascia latae and gluteus medius,[19] and either a trochanteric

osteotomy or partial detachment of the anterior portion of the gluteus medius and minimus (off the greater trochanter) are performed.[20] In the posterior approach, the surgeon enters the joint through the gluteus maximus split. The posterior hip capsule is incised, and the external rotators (piriformis, superior and inferior gemelli, and obturator internus) are detached.[21] Retrospective studies as well as clinical trials have collectively presented inconclusive results as to which method has better functional outcome.[22-24] In a conscious effort to avoid dislocation, modifications to the approaches have been proposed that repair or preserve soft tissues, such as repairing the posterior capsule incision,[25, 26] or both the posterior capsule and short external rotators.[27-30] All these methods are purported to show significant improvement in dislocation rates. Conversely, additional literature reporting conflicting results suggests that soft tissue repair has a high propensity to fail, and that repair alone does prevent dislocation. Failure rates of short external rotators were reported as high as 70% and 75%, with the majority having failed within the first post-operative day, and the rest within 3 months after the operation.[31, 32]

A large femoral head size has also been presented as a preventative measure for dislocation. Studies where only the implant is tested have determined that larger head-neck ratios have larger impingement-free ranges of motion.[33, 34] Retrospective studies, however, fail to provide statistically significant evidence that femoral head size can reduce the incidence of dislocation.[35-37] In these studies, the results were not statistically significant due to small sample sizes, or the reported decreases in dislocation rates were confounded by other experimental variables.[36]

Implant placement is another proposed dislocation risk factor which has been given a great deal of attention. In 1978, Lewinnek[38] published guidelines for acetabular cup position relative to the body's axis. Observing that excessive anteversion leads to posterior dislocation, a safe zone of lateral tilt was determined to be $40\pm10°$ with an anteversion of $10\pm10°$. Cup tilt and anteversion are illustrated in Figure 1.
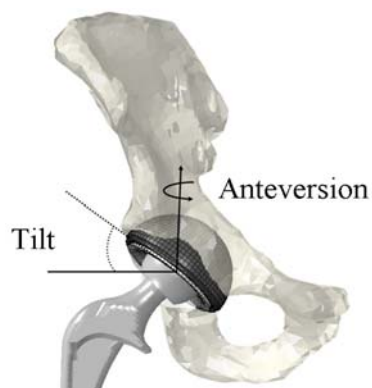
Figure 1. Schematic showing implant placement parameters.[39]

This safe zone has been supported by a later publication by Nishii et al.[40] in demonstrating a connection between low cup anteversion and posterior dislocation. Other groups reached similar concensus.[41, 42] However, the majority of the peer-reviewed literature has lacked statistical significance, with the exception of the Nishii et al. report. Conversely, other studies have reported that there is not a universal safe range for the position of the acetabular component.[43-46]

<u>1.4 Research Methods for Studying Dislocation</u>

What is missing from dislocation literature is a study where the effects of soft-tissue quality and repair, implant geometry, and implant placement have been examined together as an interactive system. Doing so would provide the means to form a unifying model of dislocation, and to craft definitive guidelines for prevention, based on a patient's unique situation. As such, retrospective clinical studies are insufficient to determine causality for a complex phenomenon such as dislocation. Poor control over confounding factors impedes the isolation of any possible cause-effect relationships.

Methods are lacking to provide a solution to this problem. *In vivo* dislocation experimentation would be unethical, while *in vitro* (cadaveric) specimen procurement is expensive, and only provides limited control over soft tissue, geometric parameters, and

sample sizes. The only method capable of providing absolute control over such a range of parameters is computational. A finite element (FE) simulation not only provides absolute control of input parameters, but is intrinsically reproducible, and can be a cost-effective method for large-scale parametric studies. For these reasons, a computational methodology has been developed in our laboratory to study impingement and dislocation. The FE model is shown in Figure 2.
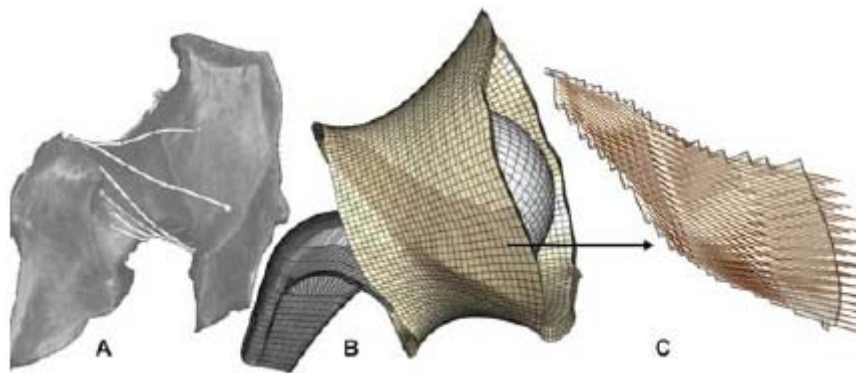


Figure 2. Native (left) cadaver hip hemi-pelvis (A), capsule representation corresponding to the FE model (B), and fiber directions of the capsule shown in detail (C).[47]

The present embodiment of the FE model implements an experimentally grounded fiber-direction-based hip capsule, allowing parametric investigation of graded levels of regional capsule atrophy, regional detachment from the capsule's femoral or acetabular insertions, of surgical incisions of capsule substance, and capsule defect repairs. Additionally, the experimental kinematics, implant geometry, and patient specific forces are fully definable.[48] Future inclusions of supplementary soft tissues such as the external rotators, piriformis, obturator internus, superior and inferior gemelli, and quadratus femoris (Figure 3), would further increase the model's biofidelity.
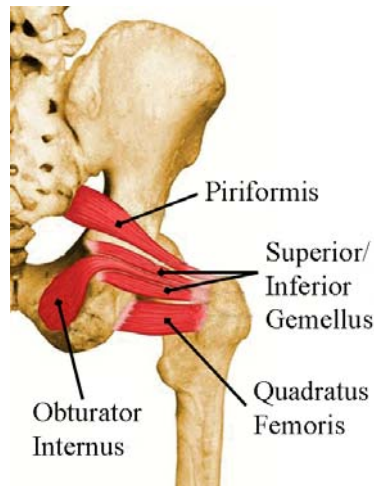
Figure 3. Drawing indicating the external rotators on a right hip.[49].

Currently the computational model represents a substantial step forward from cadaver/surrogate testing, retrospective literature studies, and hardware-only testing. The method of course also bears a burden of needing to be validated clinically and physiologically. Both theoretical and experimental validations are useful for providing a necessary level of confidence in the FE predictions. In the case of the FE model, experimental validation entails testing a cadaveric specimen with defined loading, kinematics, implant geometries and implant placement parameters. An FE model would then be created with similar parameters, ideally exhibiting similar behavior as the *in vitro* test. Having validated the FE model with physical testing results, it can confidently be used to explore implant tissue dislocation scenarios that otherwise would not be feasible to test experimentally.

Developing an experimental testing device and procedure is the subject of the present research. Advancements of an existing servo-hydraulic hip simulator, validation of the completed systems, a novel specimen preparation procedure, and use of the hip simulator for conducting FE model validation experiments will all be discussed in detail.

## 1.5 Hip Simulators

Hip simulators are not new. They have been used extensively in the last 35 years, mostly for tribology studies of hip implants. As time has progressed, so have hip simulators.  Their ability to replicate realistic joint motion, forces, and environmental conditions has dramatically increased their capacity to accurately study prosthesis wear.[50] More recently, hip simulators have been utilized in quantifying an implant's impingement-free range of motion[33, 51, 52] in order to better understand the effect that a particular implant has on dislocation rate. A noteworthy example is the 7 degree of freedom (DOF) hip joint simulator built by Kazuo Kiguchi, which has a very wide range of motion, and can impart forces and moments in all directions and about all axes. However, that hip simulator, as impressive as it may be, is severely limited for studying dislocation, as it has the capacity to test only implants. Thus, relatively few factors contributing to implant instability can be studied with that machine. Surgical approach and soft-tissue tension are all unavailable as testing parameters. To this author's knowledge, there has been only one other hip simulator designed for the specific study of hip joint instability with cadaveric tissues[53] but as of yet there have been no published plans to incorporate a hip prosthesis into that simulator. Clearly, a large void exists in cadaveric *in vitro* testing of THA component dislocation using mechanical simulators. In a move toward filling this void, the improvement of an existing hip simulator for this purpose is proposed. In doing so the research aims of creating a device and specimen procedure for use in validating the FE hip capsule model are addressed.

## 1.6 University of Iowa Hip Simulator

The hip simulator is a 4 channel, 6-DOF closed-loop servo-hydraulic hip joint motion simulator (Figure 4). The device mounts to an MTS 858 Bionix materials testing machine (MTS Systems Corp., Eden Prairie, MN) that has been upgraded from 2 to 4 hydraulic channels. The custom unit consists of two heavy-duty aluminum yokes,

mounted in series on the Bionix axial/rotary actuator. The inner yoke delivers hip flexion-extension (±55º), while the outer yoke delivers abduction-adduction (±20º).
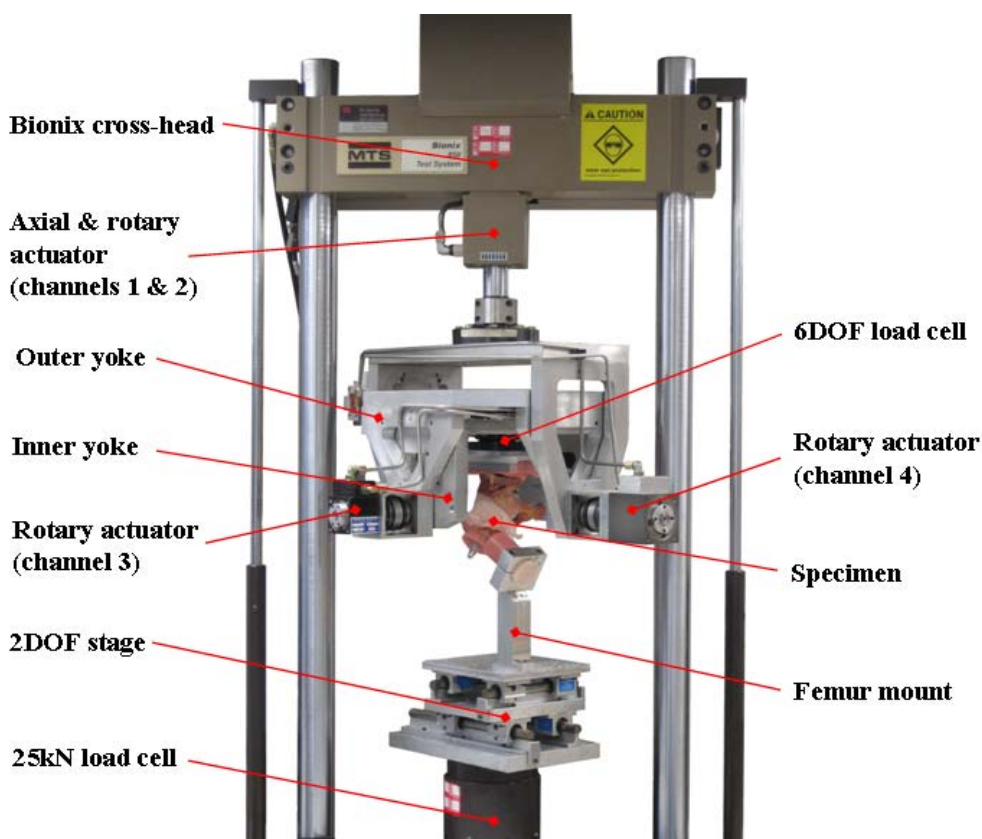


Figure 4. The hip simulator. Noteworthy components are indicated.

The Bionix's rotary channel delivers hip endorotation-exorotation (±20º), and its axial channel delivers resultant contact force magnitude. The simulator is mounted above a 2 DOF translation stage that is rigidly attached to the Bionix's 25kN axial-torsion load cell. Figure 5 shows the DOF of the machine and notable attributes. Joint motion is measured using a linear variable differential transducer for the axial displacement, a rotary variable differential transducer for endorotation/exorotation, and a variable capacitance transducer for both abduction/adduction and flexion/extension rotations. All

joint motion is controlled using the supplied MTS software, whereby simulations can be pre-programmed in a proprietary language called Multi-Purpose Testware.
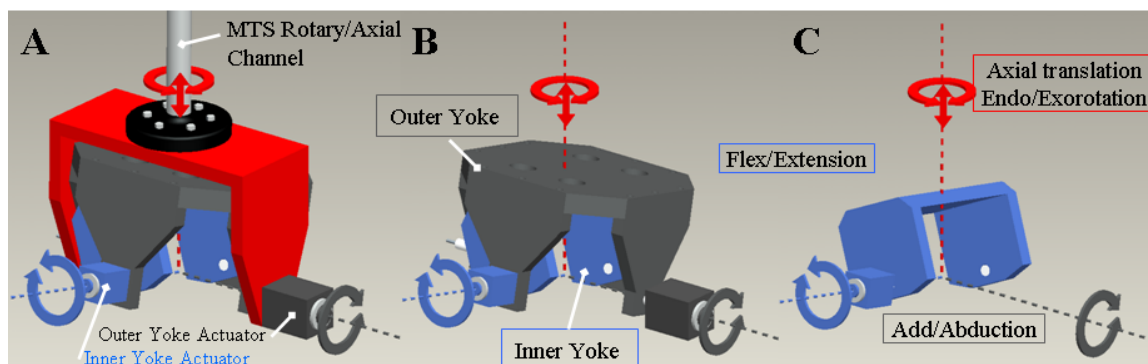


Figure 5. Schematic drawings revealing the hip simulator (A), with the support frame removed (B), and with the frame and outer yoke removed (C).

### 1.6.1 First Application of The University of Iowa Hip Simulator

The hip simulator was first used for studying the effect that implant subluxation has on the incidence of 3rd body wear[54] (Figure 6). In those studies, the center of rotation (COR) of the THA was known exactly, and did not require any procedural steps align the COR of the prosthesis with the COR of the hip simulator. Measurements of the forces and moments with respect to the THA were not required, and there was no instrumentation to do so. The motion that was simulated consisted of simplistic sinusoidal patterns, providing significant operational headroom for the rotary actuators responsible for the motion.

From conception, the hip simulator was designed to allow for the testing of cadaveric hips. However, the initial configuration, prior to this research, only allowed the testing of bare THA components, and lacked instrumentation for measuring specimen forces and moments.
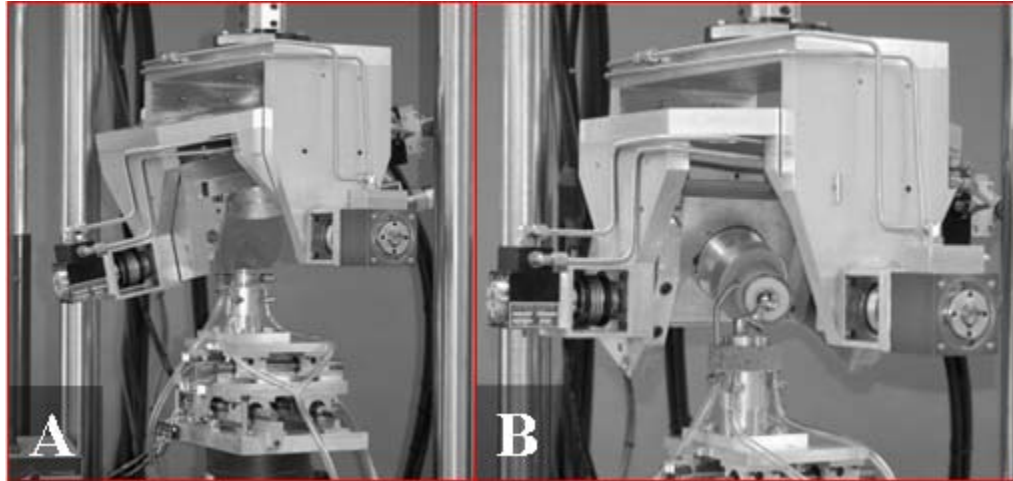
Figure 6. Photographs of the initial hip simulator configuration. The hip simulator is shown conducting a 3rd body wear experiment (A), and a close-up of the internal yoke of the hip simulator (B).

### 1.6.2 THA-implanted Cadaveric Hemi-Pelvis Testing

The objective pursued in this research is to develop the initial hip simulator into a device capable of testing a hardware-implanted cadaveric hip, for dislocation studies. A device with these capabilities would allow for evaluating capsule repair techniques aimed at lowering the risk of dislocation. The work was intended to enable the anatomically realistic impingement studies, to provide for FE validation, and to allow for future as yet unplanned cadaveric hip experiments.

The initial hip simulator needed to be upgraded to allow for the higher demands required in cadaveric testing. The addition of soft tissue and prosthesis impingement events was expected to dramatically increase the resistance to motion, and load on the hydraulic rotary actuators. Performance-enhancing modifications were necessary in order to insure accurate motion of the rotary actuators when testing cadaveric specimens. A procedure needed to be created that identifies the COR of the specimen, along with a means of placing the specimen within the hip simulator so that the COR of the specimen and that of the hip simulator were aligned. Joint forces and moments needed to be

measured during testing, and some degree of feedback was necessary to prevent damage to the device or specimen. Additionally, a motion sequence that emulated dislocation-prone kinematics needed to be defined with respect to the hip simulator's coordinate system, and programmed using MTS' Multi-purpose Testware. To this end, technical considerations corresponding to these objectives are described below.

### 1.6.2.1 Tissue Preparation

The most fundamental hurdle for cadaveric testing was developing a method that allowed an irregularly shaped object (specifically, a cadaveric hemi-pelvis) to be robustly mounted in an orthogonal-axis device (i.e. the hip simulator) such that it could support large forces and moments during testing. Polymers, with block potting for creating orthogonal mounting bases to test irregularly shaped specimens, have been used extensively for such purposes.[55-57] The specimen needed to also be easily removable, and replaceable both accurately and reproducibly. The polymer base needed to be consistent between different specimens, facilitating a well-prescribed placement procedure. Every specimen needed to be mounted in approximately the same orientation, to allow for inter-specimen comparisons to be made. Finally, neither the preparation process nor the fixation method should affect the specimen's ability to impinge, or restrict its natural range of motion. Understanding the physiological range of motion, and designing a polymer block mold to be used in creating a base to accommodate this motion, was necessary for a successful simulator outcome.

### 1.6.2.2 Instrumentation

To quantify joint forces and moments 3-dimensionally, 6 degrees of freedom (DOF) necessitate corresponding instrumentation (3 force and 3 moment measurements). This in turn necessitates the use of a single multi-DOF load/torque cell, as opposed to constructing an equivalent measuring device from single-DOF load/torque cells. For this reason, a 6 degree of freedom (DOF) load cell manufactured by AMTI (Advanced

Mechanical Technology, Inc. Watertown, MS) was purchased. The load cell is capable of measuring Fx, Fy, Fz, Mx, My, and Mz, with limits of 1100N, 1100N, 2200N, 56Nm, 56Nm, and 28Nm, respectively. By integrating the load cell into the hip simulator, the joint forces and moments could be computed, for use in quantifying the mechanical effects of soft tissues, implant geometry, and joint motion. Successful usage of a 6 DOF load cell for measuring joint forces and moments has been achieved in the Kiguchi simulator, and in other hip motion simulators as well.[34, 53, 58] The 6 DOF load cell is critical for successfully studying joint instability and dislocation events, due to its ability to measure all forces and moments accurately while occupying minimal space within the hip simulator.

Incorporating a 6 DOF load cell into the hip simulator was not without its challenges. Not only did it need to be physically integrated, it needed to not restrict specimen placement, or limit the device's range of motion. Once the load cell was integrated, specialty methodology needed to be developed for collecting and post-processing the resulting 6-channel data stream.

### 1.6.2.3 Computing the Hip Joint Center

Determining the hip COR was one of the significant computational challenges involved in the development of the hip simulator and the specimen preparation procedure. To test a cadaveric hip within the hip simulator, the specimen's joint center (JC) and the hip simulator's COR needed to be coincident. Not achieving such alignment is analogous to applying a moment to a disc, about an axis other than its COR: a larger moment is required for rotating the disc than if the moment was applied about the COR. If the JC of the specimen were mal-aligned with the COR of the hip simulator, the measured forces and moments about the JC of the specimen would be erroneous. Even small spatial alignment errors can lead to significant force and moment errors.

To reduce the amount of error attributed to mal-alignment between specimen and hip simulator, it was critical to accurately determine the spatial location of the hip JC. For the location of the hip JC to be useful, it must be referenced to a geometrical location consistent among specimens. In this context, the polymer block mold was used as an origin for which to reference the JC. As it is this polymer block mold that was used for mounting the specimen, aligning the hip JC with the COR of the hip simulator was trivial. In conjunction with an adjustable mounting system, a specimen could be placed within the hip simulator to accommodate large variability between specimens. The computational technique for computing the hip JC was adopted and modified for use from peer-reviewed literature.

Published methods for determining JC's vary appreciably depending on the intended purpose. A majority of the developments have been for applications in gait analysis, where the estimated joint/muscle/contact forces and moments are highly dependent on location of the JC (hip, knee, ankle, shoulder, etc.).[59] In computation-based methods for locating the hip JC, the joint is assumed to be spherical. Position data are captured for one, or both, of the members comprising the joint. Of various approaches surveyed, only those that used 3D motion data to determine JCs were explored, to take advantage of a Qualisys 3-camera optical motion capture system available for usage. Of these various JC locator techniques, a broad categorical approach is called the sphere-fit method.[60] A specific sphere-fit technique was ultimately chosen because of its low computational cost, high accuracy, and low sensitivity to data collection methods. In this sphere-fitting technique, optical markers are placed on both of the joint's two members. One of the two joint members is assumed to be fixed, while the other is moved throughout its ROM. During this movement, 3D position data are collected and used to fit either a single sphere (in the case of 1 marker on the moving joint member) or concentric spheres (in the case of multiple markers on the moving joint member). The center of the sphere corresponds to the joint center. The sphere-fit algorithms are most accurate when

the moving joint body undergoes a range of motion greater than 20º.[60, 61] The spherical-fit methods minimize a cost function that is equal to the sum of the difference of two quantities. The first quantity is the euclidean distance between a data point and some center c (design variable). The second quantity is a radius r (design variable). Assuming that all the data points lie precisely on the surface of a sphere having a center point c and a radius r, the resulting value of the cost function would be equal to 0. The most common sphere-fitting cost functions are below:

Equation 1. Cost functions used in solving for the hip joint center that use 3D position data of a moving joint body for their input.

**Cost Functions :**

**Single Marker**

$$S1: f(\vec{c}, r) = \sum_{i=1}^{n} (\| \vec{v}_i + \vec{c} \| - r)^2$$

**M Number of Markers**

$$S2: f(\vec{c}, r_j) = \sum_{j=1}^{m} \sum_{i=1}^{n} (\| \vec{v}_{j,i} + \vec{c} \| - r_j)^2$$

$$S3: f(\vec{c}, r_j) = \sum_{j=1}^{m} \sum_{i=1}^{n} (\| \vec{v}_{j,i} + \vec{c} \|^2 - r_j^2)^2$$

**Input data**

$\vec{v}_i$ = The $i^{th}$ data coordinate s

$\vec{v}_{j,i}$ = The $i^{th}$ data coordinate s of the $j^{th}$ marker

**Design Variables**

$\vec{c}$ = center of ideal sphere

$r_j$ = radius of ideal sphere for marker j

The accuracy of the spherical-fit methods depend upon the number of data points collected, the distance between markers (if applicable), and (inversely) on the distance between the JC and markers.[61] S1 and S2 are geometric sphere-fit models,[62] and have been reported to have poor performance when compared to S3.[63] Additionally, S1 and S2 are non-linear, and lack a closed-form solution.[64] S3, in contrast, is an algebraic sphere-fit method originally proposed by Delonge (1972) and Kasa (1976), and has a closed-form solution. This is to say that S3 can be expressed analytically with a bounded number of elementary functions. [64, 65]

From the literature reviewed, the algebraic spherical-fit model seemed the best algorithm for resolving the hip JC. It has been shown to have comparable, if not lower, error than the other techniques, it requires significantly less computation time, and it is not as sensitive to marker placement.[60, 61]

### 1.6.2.4 Computing Forces and Moments with Respect to
### the Hip Joint Center

The second significant computational challenge involves processing the 6-DOF load cell's force and moment data into physically meaningful information. Experimentally, the forces and moments of primary interest are those with respect to the specimen's JC. It is desirable to know the resisting moments referenced to the specimen, not to the load cell. Spatial transformations of the forces and moments are necessary to convert the output of the load cell from its internal reference frame, to that of the specimen. There are 3 coordinate systems that describe the system. The first is coincident with the effective origin of the load cell. The effective origin of the load cell is defined as the point where applied axial loads always produce zero moments. The second coordinate system is with respect to the pelvis. Its origin is aligned with the JC, and the z-axis, y-axis, and x-axis are equivalent to anatomical directions of superior-inferior, medial-lateral, and anterior-posterior, respectively. The third coordinate system is fixed to the femur. Like the pelvis system, the origin of the femoral coordinate system is coincident with the JC, and the z-axis, y-axis, and x-axis are equivalent to the femur's superior-inferior, medial-lateral, and anterior-posterior, respectively, anatomical directions. These three coordinate systems are illustrated in Figure 7.
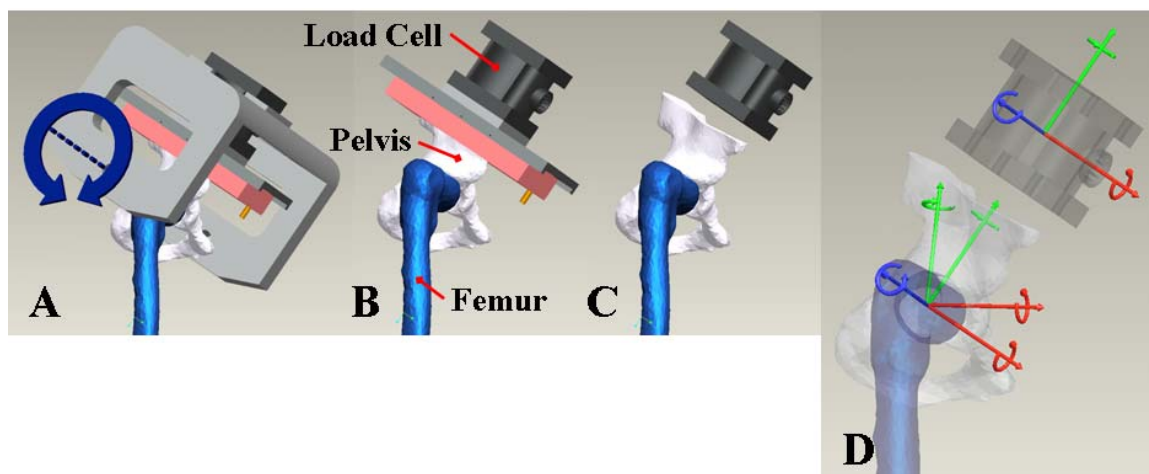
Figure 7. CAD drawings illustrating the 3 coordinate systems defined by the rotating load cell, rotating joint member (pelvis), and the non-rotating joint member (femur). The drawings begin by showing the entire inner-yoke of the hip simulator (A), how the load cell and pelvis are rigidly attached to each other (B), the two joint members and load cell (C), and the 3 coordinate systems (D).

The pelvis is attached to the 6-DOF load cell, which in turn is rigidly fixed to the inner yoke. Therefore, both load cell and pelvic coordinate systems rotate together as dictated by the simulator. The coordinate system of the femur does not rotate, and is assumed to be fixed throughout the duration of data collection. This may appear contradictory as the femur is permitted to move in its anatomical transverse plane via the x-y stage, but the purpose of transforming the joint forces and moments with respect to the third (femoral) coordinate system is to provide the forces and moments with respect to a fixed coordinate system to aid in data interpretation. It is much easier to interpret force and moment data when the reference coordinate system is static, rather than moving. To transform the forces and moments measured in the load cell coordinate system to the pelvis coordinate system, a simple translation is required. Once the forces and moments have been found with respect to the pelvis, a rotational transformation can then be used to determine the forces and moments with respect to the femur. These two transformation steps (translational and rotational) are depicted in Figure 8.
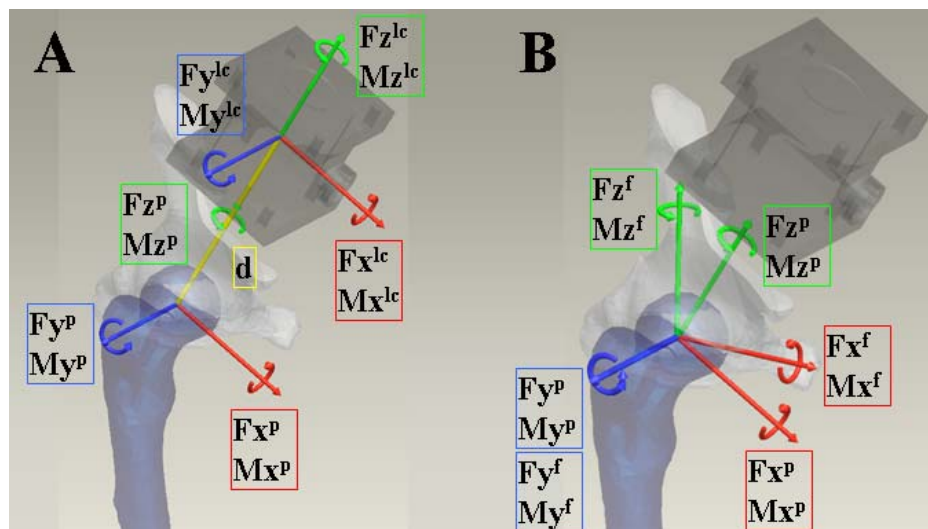
Figure 8. Schematics illustrating the two steps required to transform the forces and moments measured by the load cell to forces and moments with respect to the femur. First, the forces and moments of the load cell are translated by vector d (A). Subsequently these translated forces and moments are then rotated (by angles equivalent to rotation of the inner and outer yokes), to solve for the forces and moments with respect to the femur.

The equations for resolving forces and moments for finite rotations and translations along a known vector are well defined in many textbooks, such as Ahmed A. Shabana's book,[66] "*Computational Dynamics*". Although the relative spatial relationship between the load cell and specimen will be specific to a given specimen, a general-use formula may be constructed for use in transforming the forces and moments with respect to the load cell, to forces and moments with respect to the pelvis, and subsequently to the femur. To translate the forces and moments from the load cell to the pelvis coordinate system, the spatial relationship must first be found. In Figure 8, the spatial relationship is represented by vector d, and is determined by the placement of the specimen within the hip simulator. Because the axes of both the load cell and pelvis coordinate systems are parallel (see Figure 8-a), the forces on the pelvis and load cell are equivalent. The method for calculating the moments with respect to the pelvis coordinate system is slightly more complicated, and demonstrated in Figure 9 and Equation 2. In Figure 9, the point P is

analogous to the COR of the pelvis, where the pelvis and load cell have parallel

coordinate systems, and their spatial relationship (described by vector d) is constant.



| Measured by Load Cell: | At P: |
|---|---|
| Fx: 0N | Fx: 0N |
| Fy: 0N | Fy: 0N |
| Fz: -100N | Fz: -100N |
| Mx: 0Nm | Mx: 0Nm |
| My: 20Nm | My: 10Nm |
| Mz: 0Nm | Mz: 0Nm |
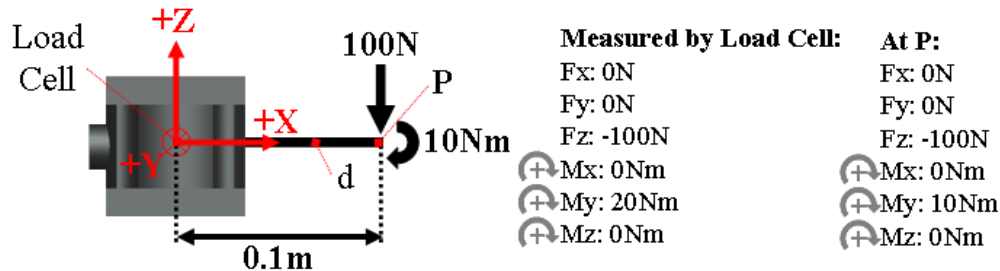
Figure 9. Diagram depicting a load and moment applied at point P of a rigid beam d, and the forces and moments measured at the origin of the load cell. Note that the load cell reports the forces acting upon it. The forces and moments do not represent a free-body diagram equilibrium.

Equation 2. The equations below describe the transforms necessary in calculating the moments and forces at point P, given the load cell output and the spatial relationship between point P and the load cell. Values from Figure 9 are used for illustrative purposes.

**Known Position, Forces and Moments WRT Load Cell :**

$$F_{loadcell} = \begin{bmatrix} 0 \\ 0 \\ -100N \end{bmatrix} \quad M_{loadcell} = \begin{bmatrix} 0 \\ 20Nm \\ 0 \end{bmatrix} \quad d = \begin{bmatrix} 0.1m \\ 0 \\ 0 \end{bmatrix}$$

**Calculated Forces and Moments WRT Point P :**

$$F_p = F_{loadcell}$$
$$M_p = M_{loadcell} - d \times F_{loadcell}$$

$$M_p = \begin{bmatrix} 0 \\ 10Nm \\ 0 \end{bmatrix} \quad F_p = \begin{bmatrix} 0 \\ 0 \\ -100N \end{bmatrix}$$

Once the forces and moments have been solved for with respect to the pelvis, these can be easily transformed to change their coordinate system from that of the pelvis to that of the femur using simple finite rotations. The orientation of the pelvis within the hip simulator can be calculated with 3 rotational transformation matrices. Each matrix (defined in Equation 3.

Equation 3) rotates a 3-dimensional vector about an axis (flexion/extension, abduction/adduction, or endorotation/exorotation) through a finite angle. Consistency of order in which the transformation matrices are multiplied together is essential, so this order is unchanged for all calculations. The first rotation is applied to the axis of the inner-yoke (flexion/extension), the second is applied to the axis of the outer-yoke (abduction/adduction), and the third is to the axis of the axial actuator (endorotation/exorotation). With this order, the orientation of the pelvis can be correctly represented given the orientation of the hip simulator, regardless of the order in which each yoke was actuated. The complete transforms needed to resolve the forces and moments with respect to the femur, given the orientation of the hip simulator (equivalent to the orientation of the pelvis and load cell), are provided in Equation 3.

Equation 3. The equations required to solve for the forces and moments with respect to the femur given the orientation of the hip simulator (equivalent to the orientation of pelvis and load cell) and the forces and moments with respect to the pelvis.

**Known Forces and Moments WRT Pelvis, and the Orientation of Pelvis WRT Femur :**

$\psi$ = **Hip Simulator Abduction/Adduction**

$\theta$ = **Hip Simulator Flexion/Extension**

$\phi$ = **Hip Simulator Endorotation/Exorotation**

$$F_{pelvis} = \begin{bmatrix} Fx_{pelvis} \\ Fy_{pelvis} \\ Fz_{pelvis} \end{bmatrix} \quad M_{pelvis} = \begin{bmatrix} Mx_{pelvis} \\ My_{pelvis} \\ Mz_{pelvis} \end{bmatrix}$$

**Calculated Forces and Moments WRT Femur :**

$$F_{femur} = F_{pelvis} \cdot \begin{bmatrix} \cos(-\theta) & 0 & \sin(-\theta) \\ 0 & 1 & 0 \\ -\sin(-\theta) & 0 & \cos(-\theta) \end{bmatrix} \cdot \begin{bmatrix} 1 & 0 & 0 \\ 0 & \cos(-\psi) & -\sin(-\psi) \\ 0 & \sin(-\psi) & \cos(-\psi) \end{bmatrix} \cdot \begin{bmatrix} \cos(-\phi) & -\sin(-\phi) & 0 \\ \sin(-\phi) & \cos(-\phi) & 0 \\ 0 & 0 & 1 \end{bmatrix}$$

$$M_{femur} = M_{pelvis} \cdot \begin{bmatrix} \cos(-\theta) & 0 & \sin(-\theta) \\ 0 & 1 & 0 \\ -\sin(-\theta) & 0 & \cos(-\theta) \end{bmatrix} \cdot \begin{bmatrix} 1 & 0 & 0 \\ 0 & \cos(-\psi) & -\sin(-\psi) \\ 0 & \sin(-\psi) & \cos(-\psi) \end{bmatrix} \cdot \begin{bmatrix} \cos(-\phi) & -\sin(-\phi) & 0 \\ \sin(-\phi) & \cos(-\phi) & 0 \\ 0 & 0 & 1 \end{bmatrix}$$

### 1.6.2.5 Choosing a Kinematic Challenge for Hip Simulator

### Cadaveric Testing

The primary research goal of the hip simulator protocol was to produce and quantify dislocation in a cadaveric hip specimen, for purposes of validating a computational hip capsule model. To this end, joint loading, tissue material properties, prosthesis placement, and joint motion between both the computational and experimental methods needed to be equivalent.

In the computational model, a variety of kinematic challenges are of interest for examining dislocation, given a set of parameters describing soft tissue, placement of the prosthesis and joint loading. Even though an approximation of the FE model can be experimentally tested using the hip simulator, perfect replication of the soft tissue and prosthesis placement is impossible. Additionally, the range of motion of the device somewhat restricts the kinematic movements that can be performed. For these reasons, the functional limitations of the hip simulator were used to direct physiologically relevant inputs for a FE model. The corresponding FE model reflected the prosthesis placement, soft tissue mechanics, and other testing parameters. Comparison of physical versus computational results then could confirm or refute the validity of the computational solution.

### 1.6.2.6 Hip Simulator Modifications

As previously mentioned, the hip simulator required a non-trivial set of augmentations in order to accommodate the testing of cadaveric tissues. Novel fixturing to support the specimen within the hip simulator needed to be both designed and manufactured. Not only did the specimen mounting method need to not interfere with the motion of the specimen or hip simulator, but the mounting also needed to allow for adjustments. Large variability between individual cadaveric hip specimens required the ability to adjust the position of the specimen within the simulator. Having a streamlined

and highly reproducible method for changing the specimen's anterior/posterior, medial/lateral, and superior/inferior position was essential to minimizing confounding placement errors associated with inter-specimen variability.

CHAPTER II: HIP SIMULATOR MODIFICATIONS, AND

VALIDATION OF INTERNAL CONSISTENCY

This chapter outlines the work performed to upgrade the hip simulator for testing cadaveric specimens. Details concerning the modifications and removal of excess mass (reduction of rotational inertia) from the existing hip simulator, fabrication of new components, and development of computational methods and their validation are provided. As a visual reference, Figure 4 shows the hip simulator in its final upgraded configuration. A cadaveric hip specimen is shown positioned within the device, to demonstrate specimen placement within the machine.
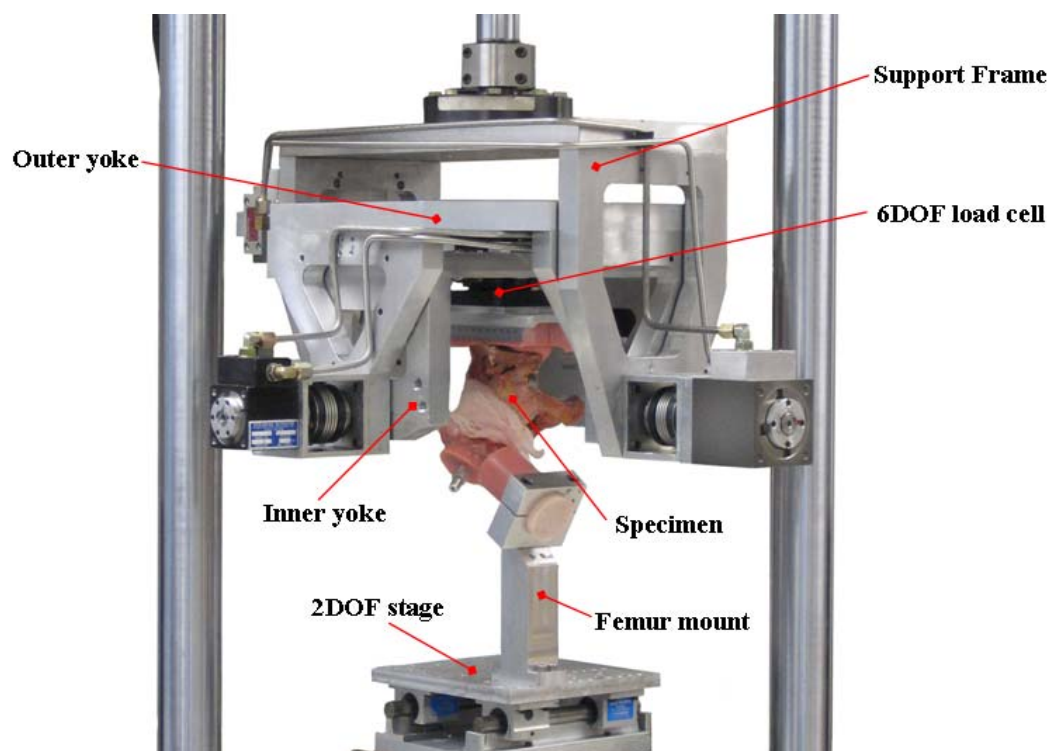


Figure 10. Close-up of the hip simulator.

<u>2.1 Removal of Excess Material, and Other Modifications</u>

The hip simulator utilizes hydraulic rotary actuators to drive the inner and outer yoke rotations responsible for the three rotational degrees of freedom: abduction/adduction, flexion/extension, and endorotation/exorotation. The resisting torques perceived by the actuators could be highly irregular during rapid rotations, especially when an off-center load reverses directions due to gravity or some other force. Based on the elementary relationship between torque, moment of inertia, and power, it is easily surmised that reducing the moment of inertia of a rotating body decreases the power required to drive a given angular acceleration. The equation below demonstrates that a decrease in the moment of inertia requires less power to accelerate a body to a given angular velocity.

Equation 4. Equation defining the relationship between the moment of inertia of a body and the power required to accelerate it.

$$\tau = I \cdot \alpha$$
$$P = \tau \cdot \omega$$

$\tau = $ **torque**
$I = $ **moment of inertia**
$\alpha = $ **angular acceleration**
$P = $ **power**
$\omega = $ **angular velocity**

The performance of the hip simulator was improved by taking advantage of the principle just described. Non-critical mass was removed from the rotating components substantially reducing their moments of inertia about all three rotational axes. Figure 11 shows the calculated change in moment of inertia for each rotational axis for the assembled hip simulator.
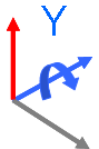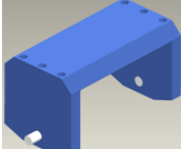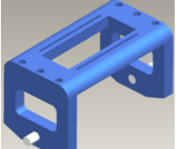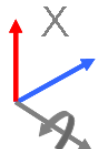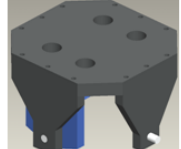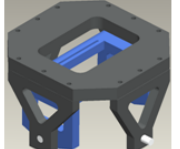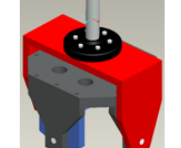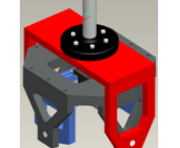
| Axis | Previous | Upgraded | Reduction in Moment of Inertia |
|------|----------|----------|--------------------------------|
|  Y |  |  | 17.2% |
|  X |  |  | 13.1% |
|  Z |  |  | 19.7% |

Figure 11. Illustration of the mass reduction of the hip simulator components and the percent reduction in moment of inertia per axis of rotation.

By removing a total mass of 9kg, an average moment of inertia decrease of 17% was observed for each rotation axis, thereby increasing the effective power of the hip simulator by nominally 17%. The effects of these improvements afford improved dynamic control, which was fundamental to specimen motion simulations.

In the process of upgrading the hip simulator from its initial state to a configuration capable of testing cadaveric specimens, a substantial number of existing hardware components also required modification. Many of these alterations involved the hip simulator's instrumented 2 DOF stage. The stage is part of the femoral mounting system. It allows for transverse movement of the femur, permitting dislocation or subluxation if necessary. Linear potentiometers were affixed as displacement transducers, allowing the MTS system to record transverse motion of the femur during testing.

Both the electrical instrumentation and physical attributes were changed to improve performance and practicality. Electrically, a dedicated 10V regulated power supply was added to provide an excitation voltage for the displacement transducers, and

10kΩ resistors were put in series with the MTS inputs, to protect from over-currents. Physically, three significant changes were made to the x-y table. The linear bearings responsible for translations in the y-direction were moved inward (towards the x-z datum plane) to increase the translational range of motion from 23mm to 50mm (Figure 12).
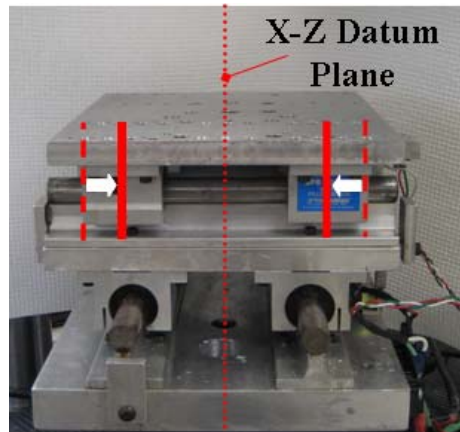


Figure 12. Photograph of the x-y table demonstrating the initial versus upgraded positions of the linear bearings. By mounting them more medially, the specimen range of motion was increased substantially.

New mounting positions for the x-direction potentiometer were also added, to increase the effective range of motion. In addition, tapped holes were added to the top plate of the x-y stage, to provide a means of attachment for the femur mount. These holes spanned the entire width, to accommodate both right and left specimens, and to provide greater flexibility in medial-lateral placement of the femur mount. These modifications are shown in Figure 13, below.
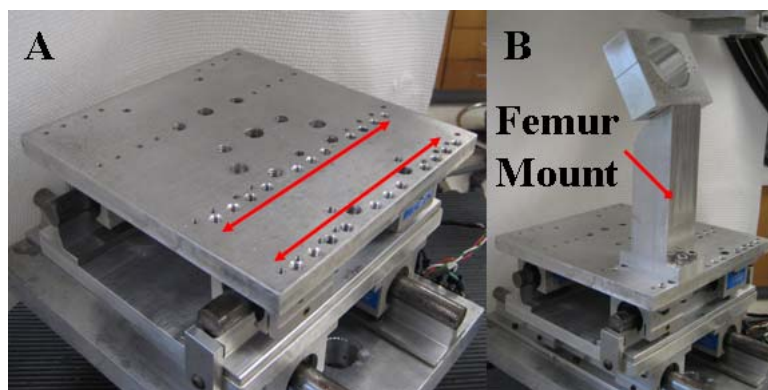
Figure 13. Photographs showing the new femur mount mounting holes (A) added to the x-y table, and how the femur mount attaches to the x-y stage (B).

## 2.2 New Component Fabrication

In the process of upgrading the hip simulator, various components needed to be re-built. A means of specimen attachment and rigid fixation, along with specimen position adjustability, were considerations that had not been addressed in the preliminary hip simulator. More than twenty individual components required manufacturing, with the total quantity of parts involved numbering more than forty. Computed Numerically Controlled (CNC) machines (a HAAS Tool Room Mill 1 and a HAAS Precision Collet Lathe) were utilized to machine these new parts. Materials used were alloy 6061 aluminum, alloy 303 austenitic stainless steel (SS), alloy 353 brass, and ultra high molecular weight polyethylene (UHMWPE). Major new components are described below, beginning with the position locking system (Figure 14). In each description, the respective design considerations, material composition, and special manufacturing considerations are detailed where applicable.

### 2.2.1 New Hip Simulator Components

During cadaveric testing, it was sometimes necessary to perform surgical procedures, and to adjust specimen placement within the simulator while the hydraulics

are engaged. In order to maintain a high level of safety, a novel locking system was developed to prevent the hip simulator from moving unintentionally.

The locking assembly (Figure 14) involves a mounting bracket machined from 76.2mm square extruded aluminum tubing. This bracket replaced a shallower version, to create space for the newly implemented locking mechanism. The bracket attaches to the support frame and to the outer yoke of the hip simulator. When the lock mechanism is engaged, the shaft is prevented from rotating. The bracket also supports the angular displacement transducer.

The two-part locking mechanism was machined from a single piece from aluminum and then separated once the central hole was bored for the diameter of the shaft. The two halves of the locking mechanism are brought together with two 3/8-16 cap screw bolts. The shaft was machined on the lathe from SS. The axles were extended in length from their previous counterparts, to provide enough circumferential surface area for the locking mechanism to engage.
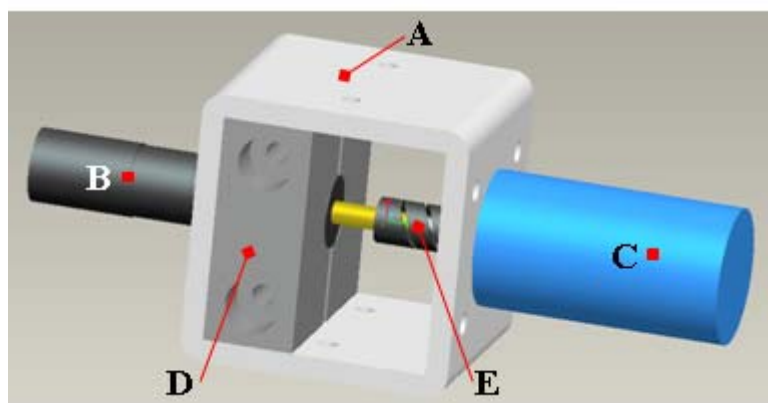


Figure 14. Schematic of the locking system for both the abduction/adduction and flexion/extension axes. The bracket (A) is mounted to the hip simulator supporting the constituent components: shaft (B), Angular Displacement Transducer (ADT) (C), lock (D), and flex coupler (E)

Space within the innermost yoke of the hip simulator was very limited. In addition to housing the specimen itself, the load cell needed to be accommodated. To provide enough room for the load cell and specimen, it was necessary to mount the load cell above the top surface of the inner-yoke top plate. This necessitated redesigning the inner-yoke top plate (Figure 15), to provide features compatible with the load cell. This mounting configuration is demonstrated in Figure 16-b. The new inner yoke top plate provided greater latitudes for initial specimen mounting, and allowed for larger size pelves to be placed within the hip simulator. By mounting the load cell in this position, the allowable specimen height (measured from the JC to the most posterior point anatomically) was increased by 40mm. The mounting position of the specimen in the medial-lateral direction was determined by load cell placement within the opening of the inner yoke top plate.
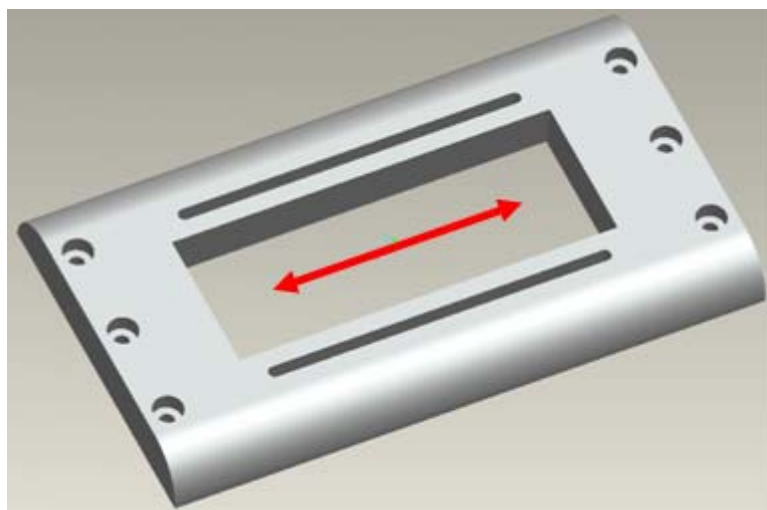


Figure 15. Inner yoke top plate. The red arrow illustrates the flexible mounting system for the load cell, allowing variable lateral positioning.

The load cell mounting brackets (Figure 16-a) supported the load cell from the internal surfaces, as opposed to the outer, more traditional mounting surfaces of the load

cell. This design was adopted for two purposes: to provide the specimen maximal space, and to minimize the amount that the load cell protruded past the top surface of the inner yoke top plate. Excessive protrusion would reduce the ROM of the innermost yoke, by reducing clearance between the protruding load cell and the outer yoke during rotation. In the upgraded state (Figure 16-b), the load cell position provided sufficient specimen versatility in the superior/inferior direction, but reduced the ROM of the innermost yoke from ±100º to ±55º. This reduction in rotation range was compensated for by mounting the femur in an adjustable offset position. With this tactic, the effective range of motion became ±115º.
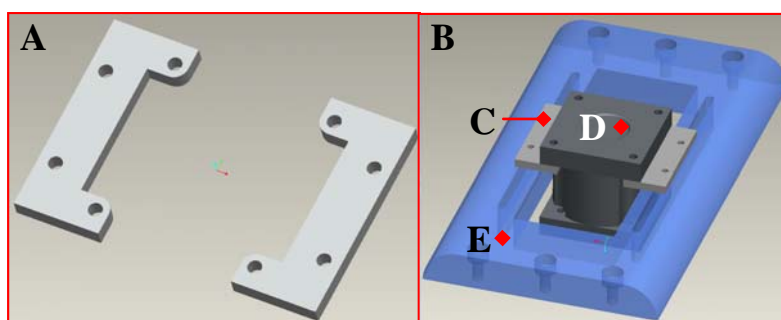


Figure 16. Schematics depicting the load cell mounting brackets (A) and their usage (B). The load cell brackets (C) rigidly fix the load cell (D) to the inner yoke top plate (E).

The specimen mounting plate (Figure 17-a) was designed to provide anterior/posterior translational adjustability for specimen placement within the hip simulator. Similarly to the adjustability of the load cell in the medial/lateral direction, the specimen mounting plate permitted the polymer block mold of the specimen to vary ±25mm from its center in the anterior/posterior. The specimen was bolted to the plate using custom nuts (not shown) that slid within the four slots. The thickness of the plate was kept minimal (7mm), again to provide the greatest amount of space for the specimen.
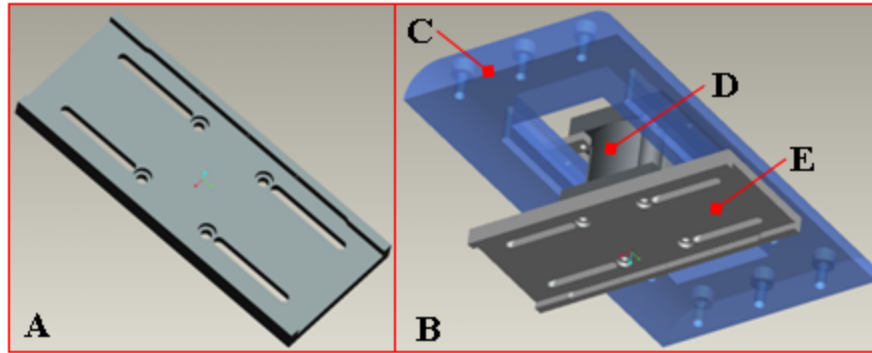
Figure 17. Specimen mounting plate, shown isolated (A) and with its surrounding components (B). The specimen mounting plate (E) is shown attached to the load cell (D) within the inner yoke top plate (C).

Purpose-sized spacers were used to change the specimen's superior/inferior placement within the hip simulator. The spacer thicknesses were chosen to provide sufficient placement resolution, while not degrading the structural integrity of the load cell and specimen mounting plate attachment. The various spacer thicknesses allowed the specimen's superior/inferior placement to vary between 50mm to 0.635mm, with increments of 0.635mm. The placement resolution afforded by the spacers was approximate to the placement resolution of the specimen in the anterior/posterior and medial/lateral axes.

The spacers were machined from flat unpolished aluminum with a thickness tolerance of ±0.051mm, ±0.102mm, ±0.102mm, and ±0.203mm for the 0.635mm, 1.27mm, 2.54mm and 6.35mm spacers, respectively. Four 6.35mm spacers were machined, along with 8 2.54mm, 8 1.27mm, and 8 0.635mm.
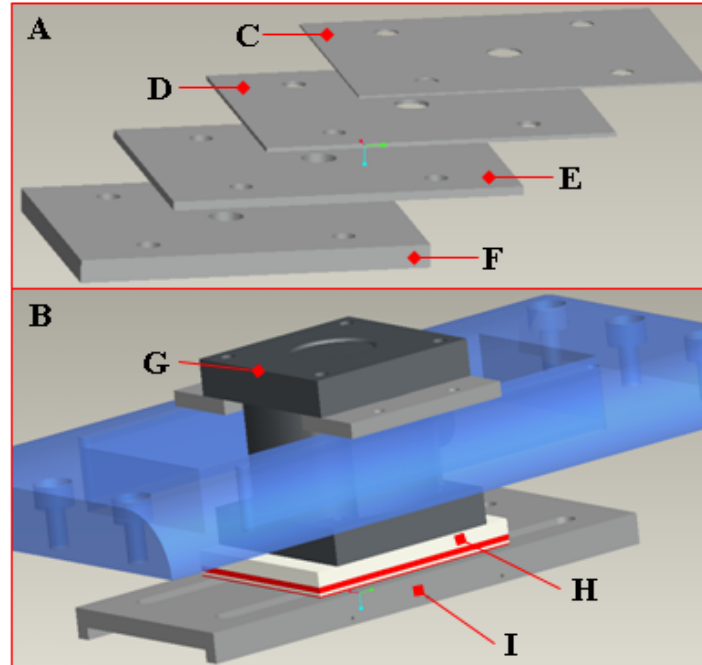
Figure 18. Spacers (A) and their application (B). In graphic A, the different spacer thicknesses are shown. The thicknesses are 0.635mm (C), 1.27mm (D), 2.54mm (E), and 6.35mm (F). In graphic B, four spacers of different sizes are shown in alternating colors (H) in between the load cell (G) and specimen mounting plate (I).

The femur fixture assembly consisted of two main components. The distinct parts are shown in Figure 19-a. The top component (C) clamps to the (PMMA potted) femur, while the bottom post (D) attaches to the hip simulator's x-y stage. The top component can attach to one of two surfaces of the bottom post. The two surfaces apply a flexion offset to the femur of either 45º or 60º. This offset allows for more versatile range of anatomical motion.  Flexion range is -5º to 110º with the 60º offset, or -10º to 100º with the 45º offset. Both ranges offer significantly more capacity in reproducing physiologic motion challenges than would otherwise be possible (±55º of flexion) without an offset. Graduated rotation reference marks were etched into the outer surface of the top component. These reference marks were used to ensure that femoral internal-external

rotation was consistent between specimens, and/or to prescribe an internal-external rotation offset to the specimen during testing.
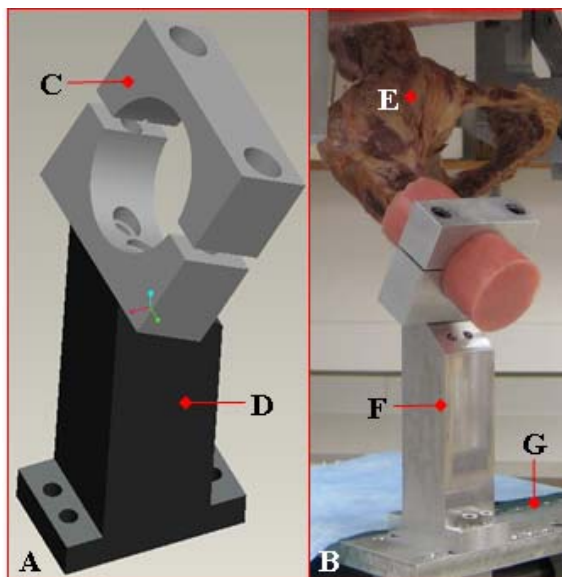


Figure 19. Schematic of the femur fixture assembly (A) and a photograph of it in use in the hip simulator (B). In the photograph, the femur fixture assembly (F) is attached to the x-y table (G) below, and to the femur of a cadaveric specimen (E).

The potting box (Figure 20) used for creating cadaveric hemi-pelvis polymer mounting blocks was made from 12.7mm thick aluminum stock. Twelve stainless steel 25mm long 8-32 cap screws were used in its assembly. The size and shape of the potting box were chosen to provide an unobtrusive base within which to mount the specimen. The width fits the internal slot of the specimen mounting plate. This restricted the specimen to only one translational degree of freedom, thus minimizing un-desired specimen positioning variability. The shorter wall of the potting box allowed the body of the pubis to protrude out of the potting box.
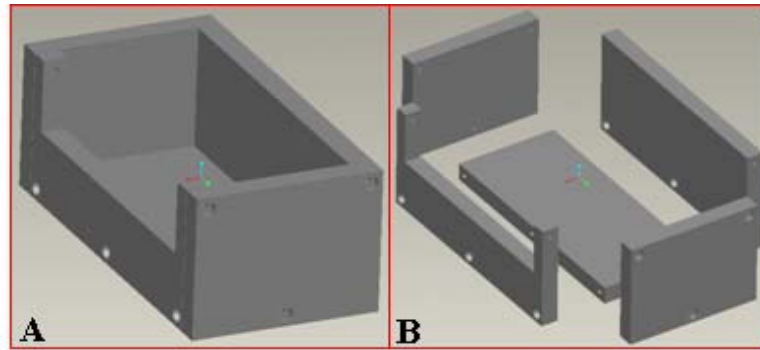
Figure 20. Graphics of the aluminum potting box assembled (A) and disassembled (B).

### 2.2.2 Fabrication of Components used in the Transpelvic Implantation Procedure

The transpelvic implantation procedure is an experimental protocol for surgically placing THA hardware within a specimen, without violating the hip capsule. Preserving the structural integrity of the hip capsule allowed for its mechanical contribution during dislocation to be quantified. The procedure was used to replicate specimen testing configurations that were modeled computationally, so that the computational model could be tested experimentally, providing physical validation of the FE model.

Figure 21 illustrates the transpelvic procedure. The procedure is described in greater detail in Chapter 3, Section 4.

The following components were fabricated for the transpelvic procedure. These involved either hardware added to the specimen (collar, liner insert, etc.), or hardware designed to assist during the procedure.
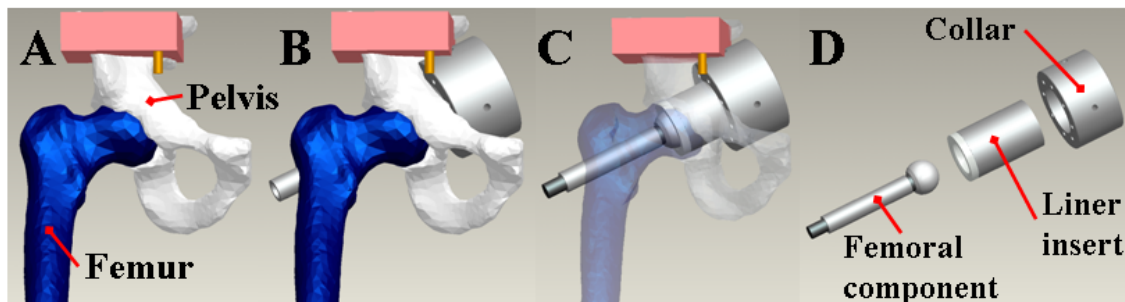
Figure 21. Schematic demonstrating the concept of the transpelvic procedure. The procedure begins with a prepared specimen (A). A hole along the axis of the femoral neck is made for the femoral component, and a larger hole is made in the pelvis to gain access to the joint (B). The femoral component and liner insert are added, reproducing normal joint mechanics (C). The three main hardware components are shown together (D).

Accurate joint orientation is highly dependent on hardware placement. The drill guide shown in Figure 22 fit over the 6.35mm drill bit aligned with the axis of the femoral neck. While aligned with the drill bit, the drill guide was used to affix a peritoneal-side collar (Figure 23). Once that collar is affixed, the peritoneal-side hole can be made using an appropriately sized hole-saw. The alignment between the drill, drill guide, and collar ensures that the sawn hole is nominally normal to the opening plane of acetabulum, and centered over the head of the femur.

The drill guide was machined to a finished diameter of 41.11mm, using the HAAS Precision Collet Lathe. This finished diameter was 0.17mm less than the internal diameter of the peritoneal-side collar. This clearance was calculated based on standard class I shaft-hole tolerances.
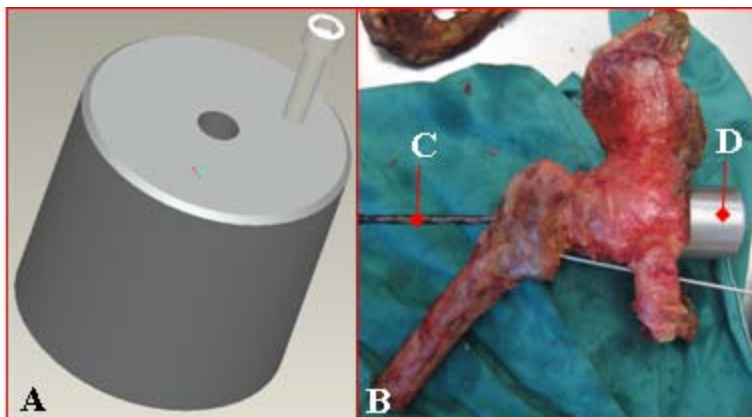
Figure 22. Schematic of the drill guide (A) and picture of the drill guide being used with a cadaveric specimen (B). The drill guide aligned the pelvis-side hole by fitting over the 6.35mm drill along the femoral neck in the transpelvic procedure, described below.

The peritoneal-side collar served three purposes. First, in preparing the specimen for experimentation, the collar was used to guide a 41.28mm hole saw in cutting through the pelvis, nominally normal to the opening plane of the anatomic acetabulum, and centered above the femoral head. Second, the collar was used for supporting the specimen while it was being worked upon (the collar fit into a larger supporting ring that securely held the specimen at a convenient height and position). Third, the collar held the UHMWPE acetabular liners and custom aluminum backing inserts (Figure 24) in place during testing. Radially aligned set screws on the circumference of the collar secured the inserts, providing a straightforward method to alter the orientation or to replace the acetabular component liner within the joint.

The collar's outer diameter was turned to 69.3mm, allowing it to be inserted into the work-supporting ring, again conforming to class I hole-shaft tolerance. The internal diameter was milled on the HAAS Tool Room Mill, where the radial bolt hole pattern was subsequently created. The holes were sized to fit size-6 self-drilling dry-wall screws. The circumferential set screws were 20threads/inch and were brass tipped, to prevent damaging the liner inserts.
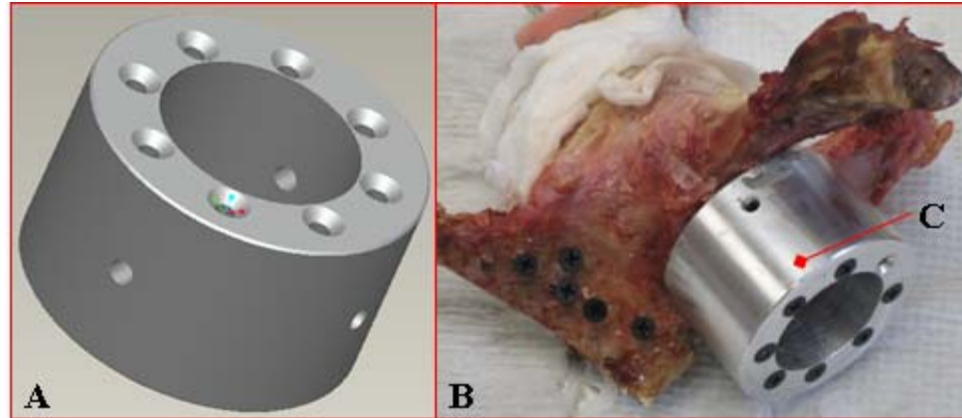
Figure 23. Schematic (A) and in-use photograph (B) of the collar.

Machining of the liner inserts was done in a four part process. The process began by turning the outer surface of the aluminum backing (Figure 24-D) 2mm greater than the final dimension of 41.28mm. This was done to allow sufficient material for a final finishing pass in a last step. In the second step, a partial hemisphere was machined into one end of the aluminum backing. The poly-liner (Figure 24-C) would later be inserted into this machined cavity. Three bolt holes were subsequently machined to provide a means of holding the poly-liners and aluminum backings together. Once the poly liner and aluminum backings were bolted together, the entire assembly was turned on the lathe to the final dimension. This final dimension conformed to standard class I shaft-hole tolerance, providing a smooth fit within the peritoneal-side collar.
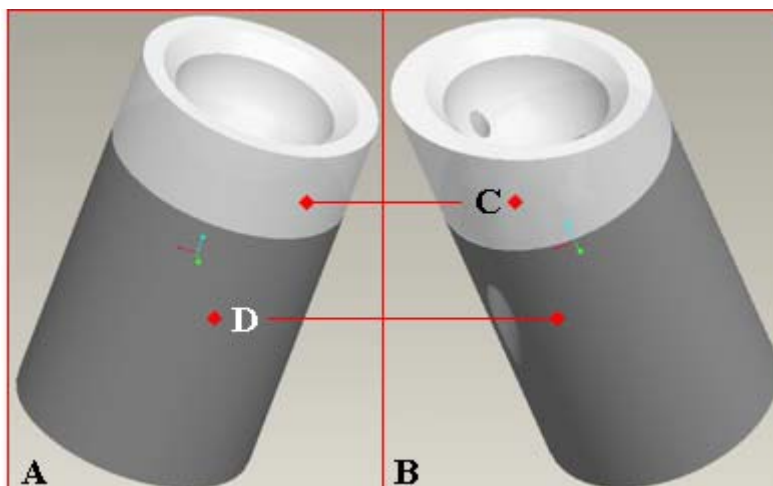
Figure 24. Schematics of the neutral cup insert (A) and a 20º cup insert (B). The liners
(C) were machined from DePuy Enduron polyethelene, while the backings
(D) were aluminum.

## 2.3 Computational Methods

The computational methods developed to capture and post-process load cell raw
data and compute the hip JC of rotation are next described.

Virtual instrumentation of the load cell was necessary for establishing a way for
the MTS control system to read in the load cell data stream. This was accomplished using
the LabView graphical programming language, while the optimization and data
processing procedures were carried out in the MATLAB environment. LabView's
manufacturer, National Instruments, provides near turn-key hardware designed
specifically for the LabView programming language. Significant time and energy were
saved in utilizing LabView, in combination with corresponding data acquisition
hardware, to implement virtual instrumentation of the load cell. An available multi-
channel signal conditioner and amplifier (System 5000) were also utilized in
instrumenting the load cell.

### 2.3.1 Load Cell Virtual Instrumentation

The MTS system that controlled the servo-hydraulic actuators had multi-purpose digital and analog inputs/outputs. When the 6 DOF load cell was initially added, it was thought that 6 of the MTS' analog channels would be utilized in reading the load cell by means of analog voltages. However, the existing multi-channel signal conditioner (System 5000) manufactured by Vishay did not have analog voltage outputs. The System 5000 was independently controlled by its own computer and proprietary software. It would have been possible to collect the load cell data separate from the MTS data collection system (resulting in two separate data files in two separate computers). However, this would have resulted in asynchronous data, and would have prevented the use of data limits by the MTS computer to protect the load cell, or use load-based feedback loops during specimen testing.

In order to allow the two systems to communicate, a collection of programs (VI's) were written in LabView to access the System 5000, and to output the force and moment values provided by the System 5000 as analog voltages to the MTS computer. To achieve this, a Dell Inspiron laptop computer was fitted with a National Instruments high-speed analog output PCMCIA card (NI DAQCard-6715). The card provided 8 ±10V 12-bit analog outputs, with a maximum update rate of 1 sample/millisecond. This configuration was the most cost-effective, given the required number of independent analog voltage outputs. Within LabView, the custom set of VI's were written to coordinate data exchange between the laptop computer and the signal conditioner, to convert from strain to calibrated units of force and moment, to compensate for cross-talk (characteristic of multichannel load cells), and to produce six unique ±10V scaled outputs. The outputs were subsequently read by the MTS computer. Sampling rates were limited to 50 samples per second. Although this was less than what is possible with the native System 5000 StrainSmart© software, 50 samples per second was confirmed by the manufacturer as the

maximum possible rate, given the method adopted for communication between the LabView VI and System 5000.

The LabView VI's read the data stream from the System 5000. Communication was done serially, with the incoming data stream consisting of six 15-bit signed numbers, one for each force and moment channel. To correctly calculate a scaled output, the excitation voltage (V), amplifier gain (mV/V), and channel sensitivity ($\mu V \backslash V_{excitation} * N$ [or Nm]) were required for each channel. The data stream was also corrected for cross-talk utilizing a "cross-talk" matrix. The values for this matrix were provided by the load cell manufacturer. These values were unique to the specific load cell used in the hip simulator. Cross-talk is a phenomenon of multi-channel load cells where the direction of force of the output is different from the direction of force being measured.[67] For example: if a load were applied to a load cell equally in the x- and y-direction, a load cell experiencing cross-talk would provide an output indicating that the load was not applied equally to both the x- and y-axes. The "cross-talk" matrix corrected for this effect by adjusting the sensitivities of each channel.

### 2.3.2 Joint Center Determination Algorithm

An accurate spatial determination of a specimen's JC was a requirement that all subsequent procedural steps relied upon. From specimen placement within the hip simulator, all the way through to joint force and moment determinations, experimental success was dependant upon an accurate JC solution. The program created to compute this was written in MATLAB R2009a. The necessary inputs included 4500 3D position coordinates of no less than 4 optical markers (3 on the femur and 1 as a fiducial). The data were captured at a rate of 100 samples per second for 45 seconds, using a Qualysis 3-camera motion capture system. The height of the fiducial, unique to a given specimen (Figure 25-b) was also required for computing the hip JC.
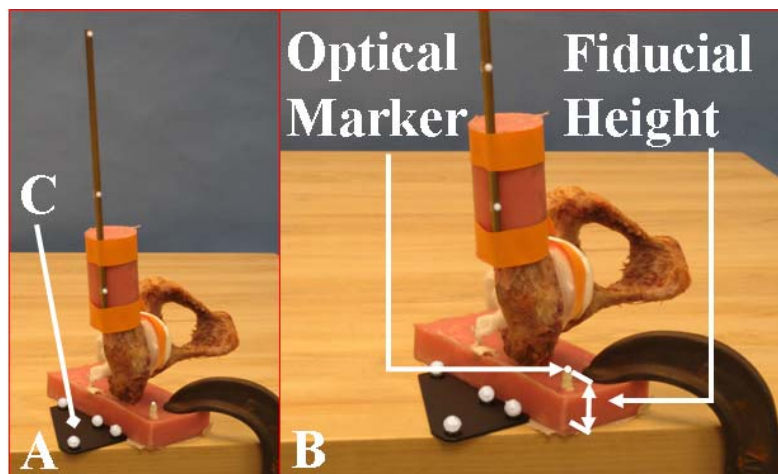
Figure 25. Photographs of a potted cadaveric specimen during motion capture. In photograph A, the calibration plate (C) is shown that aligns the data capture reference frame with that of the PMMA base. In photograph B, the fiducial marker and its height are shown in close-up.

This fiducial marker consisted of a single optical marker that represented a known position on the hemi-pelvis' PMMA base. All other markers were placed along the long axis of the femur. The optical motion capture system was calibrated such that the measurement coordinate system was parallel with the specimen's coordinate system, which in turn was determined by the PMMA base.

Given these position data, a spherical surface was fit to the positions of a single femur marker. This process was repeated for the other 3 (or more) femoral markers. The optimization algorithm required initial values of the center (*centerX*, *centerY*, & *centerZ*) of the ideal sphere, as well as a radius (*r*). These values were then incrementally altered during the optimization process, until the cost function had been minimized. The initial values were constant for all specimens, defined as the center of the x-y plane of the PMMA block, at a height equal to that of the fiducial. The cost function is defined below.

Equation 5. Cost function definition used to resolve the hip joint center using 3D position data captured using a Qualysis 3-camera optical motion capture system.

**Cost Function to be minimized :**

$$error = \sum_{i=1}^{4500} ((femurX_i - centerX)^2 + (femurY_i - centerY)^2 + (femurZ_i - centerZ)^2 - r_1^2)^2$$

**Input Data :**

$femurX_i = \mathbf{i^{th}\ x\text{-}coordinate}$

$femurY_i = \mathbf{i^{th}\ y\text{-}coordinate}$

$femurZ_i = \mathbf{i^{th}\ z\text{-}coordinate}$

**Design Variables :**

$centerX = \mathbf{x\text{-}coordinate\ (center\ of\ ideal\ sphere)}$

$centerY = \mathbf{y\text{-}coordinate\ (center\ of\ ideal\ sphere)}$

$centerZ = \mathbf{z\text{-}coordinate\ (center\ of\ ideal\ sphere)}$

$r = \mathbf{radius\ of\ ideal\ sphere}$

This particular cost function differs from published methods in that each marker was processed individually, rather than in concert, to create concentric fitted spheres. Preliminary data suggested that computing them individually reduced the final solution error. The center of rotation solution for each femoral marker was used in a weighted average, based on their distance from the JC, to compute a final solution. This method is supported by literature stating that the accuracy of the solution is inversely proportional to the marker's distance from the joint center.[60, 61]

The method of 'steepest descent' was used to minimize the above cost function. In this procedure, the partial differentials of the cost function were found with respect to each design variable, and the design variable that most lowered the error was incremented or decremented by 0.01 mm. This was repeated until a change in a design variable no longer decreased the value of the cost function. Using the JC computed from the optimization process, the placement of the specimen within the hip simulator was

computed. The placement of the specimen was defined as the x-, y-, and z-placement positions which corresponded to the anterior-posterior, medial-lateral, and distal placement of the specimen. This computed placement of the specimen represents the position of the specimen where the CORs coincide.

The hip was assumed to be an ideally spherical joint, an assumption generally accepted in resolving the hip JC.[61, 68-70] This assumption holds reasonably well for disease-free hips, but may lose its accuracy if the hip has a limited range of motion[71] or if there are bone deformities. The specimens tested in the present series either had surgically placed THA hardware, or were deformity-free, justifying this assumption.

### 2.3.3 Load Cell Data Stream Processing

The force and moment data captured during experiments by the MTS system were with respect to the local coordinate system of the load cell. As the point of interest was not at the load cell but rather at the JC, it became necessary to change the spatial reference frame of the initially measured forces and moments to that of the JC. Further transformations were in turn made to change the reference frame from the (rotating) pelvis to that of the (non-rotating) femur. All three spatial reference frames are demonstrated in (Figure 26). The transformations had the advantages of easing data interpretation by the user, and of making the final reference frame identical to the MTS system. All data manipulations were done in the MATLAB programming language, chosen for its convenient/powerful matrix computational abilities.
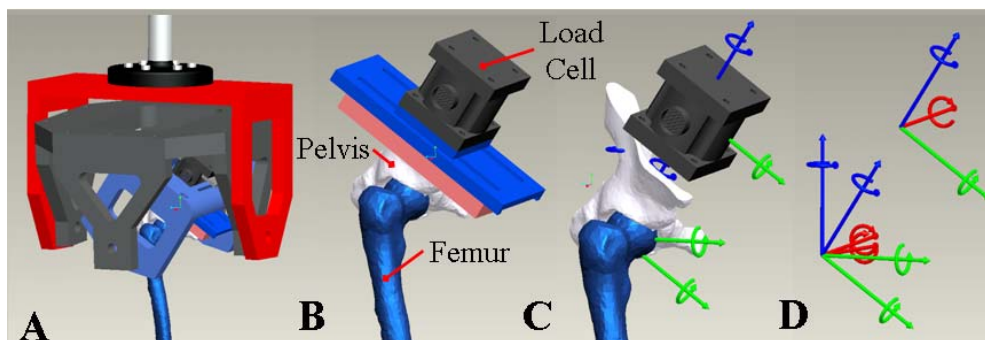
Figure 26. Rendered CAD drawings of the hip simulator (A) demonstrating the location of the three individual reference frames (D), The load cell, pelvis and femur (B) are shown with their respective imbedded coordinate systems (C) for reference.

Data necessary to compute forces and moments with respect to the hip JC included all six load cell force and moment components, the specimen position within the hip simulator (not the position of the JC, but rather the position of the PMMA base), and the hip simulator orientation (flexion/extension, abduction/adduction, and endorotation/exorotation). These data were provided in the MTS system's *.dat output file, and required no additional modifications before processing. Once the data had been loaded into the MATLAB workspace, they were cropped based on a predetermined starting condition. This action removed timing variability between experimental runs, facilitating direct comparisons. If this had not been done, each experimental run would have had a different amount of time between the start of data collection and the instant when joint motion began. This inter-specimen variability was due to the difference in time that was required to add an axial load to the joint prior to testing. The rate at which the axial load was applied was specified and constant for all specimens, but subtle movements that occurred while the specimen was being loaded could add additional time to this process.

During processing, data transformations were made for each set of data points at every time step. To convert from the load cell to pelvis reference frames, the vector $d$

connecting the two spatial frame origins was calculated (Figure 27-a). The load cell

forces and moments were then rotated $+\alpha$ about the y axis, making the z axis and vector $d$

parallel.
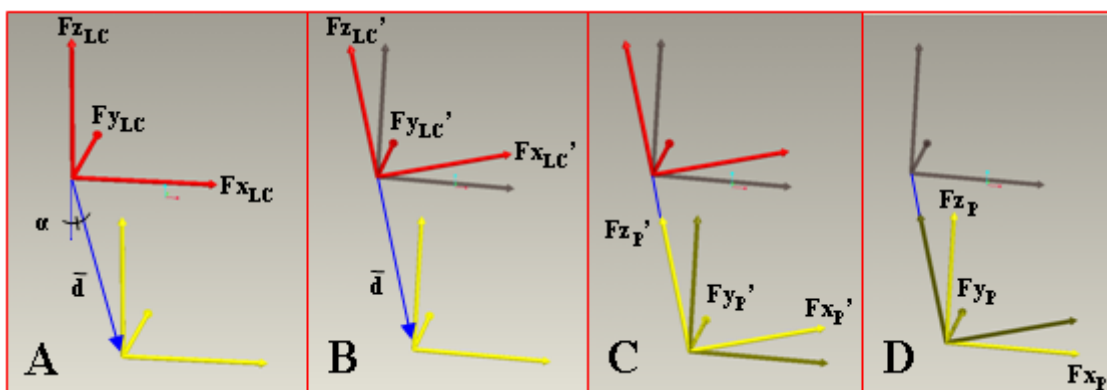


Figure 27. Schematics of the four analytic steps used to resolve forces with respect to the specimen's joint center. First the vector d and angle α were found (A). The load cell's forces were then rotated about the y-axis by positive α (B). Using vector d and the load cell's moments, intermediate forces with respect to the pelvis were found (C). Lastly, the intermediate forces were rotated through an angle of −α (D).

The forces and moments in the pelvis reference frame were calculated in

accordance to the general-use computation method outlined in Chapter 1.4. The newly

calculated pelvis forces and moments were then rotated $-\alpha$ about the y axis, to correct for

the initial rotation. To make the final transformation from the pelvis reference frame to

the femur reference frame, the forces and moments were multiplied by three successive

transformation matrices (set forth in Chapter 1.4). Each transformation matrix rotated the

forces and moments about a single axis corresponding to the orientation of the hip

simulator at the time step being evaluated. The rotated forces and moments that were

once with respect to the pelvis were then with respect to the femur. The program's final

task consisted of saving the computed results and supplementary information to an Excel

file. Additional information included superior/inferior displacement, axial force measured by the MTS hip simulator's 25kN load cell, anterior/posterior and medial/lateral displacements of the femur, and the hip simulator orientation (flexion-extension, abduction-adduction, and endorotation-exorotation).

### 2.4 Load Cell Data Stream Processing and Center of
### Rotation Validation: Experimental Methods and Results

Validation experiments were designed in order to confirm that the output of each algorithm step was internally correct. Specifically, the load cell data stream processing and the center of rotation algorithms were tested to evaluate their level of accuracy. Each experimental method is followed by its respective results.

### 2.4.1 Load Cell Data Stream Analysis Processing
### Validation: Experimental Methods

The load cell data stream post-processing algorithm was tested to confirm its accuracy and to provide a means to correct any coding mistakes. The importance of accurately transforming the load cell forces and moments to values defined with respect to the specimen's JC justified substantial effort to ensure that the corresponding programs functioned as intended.

A testing method was designed to parallel the actual experimental procedure. Within the hip simulator, the load cell was fixed off-axis, and a hanging mass was attached to the load cell so that the hip simulator's rotational center and the point of mass suspension were coincident (Figure 28).
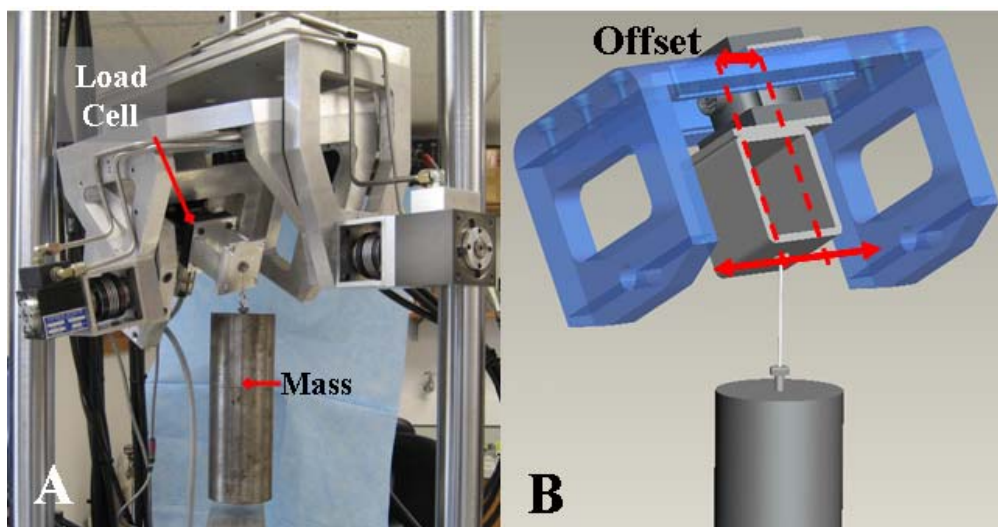
Figure 28. Photograph and schematic showing the experimental setup. The hanging mass and load cell are noted in the photograph (A) and the load cell offset is demonstrated in the schematic (B).

The hip simulator was commanded to oscillate about its abduction/adduction and flexion/extension axes with amplitudes of 13º and 60º, respectively, at a frequency of 0.4Hz. All six output channels of the load cell were sampled at 50Hz, for 40 seconds. The combination of the sinusoidal motion and the hanging mass provided led to raw load cell output for all six channels: $F_x$, $F_y$, $F_z$, $M_x$, $M_z$, and $M_y$. Due to the coincident rotational centers of the hanging mass and hip simulator axes of rotation, the forces and moments with respect to a fixed global coordinate system (given its origin at the hip simulator's axes of rotation) should be zero, except for a single force in the negative z-direction, equal to the weight of the hanging mass. This specific experiment provided a test to validate the load cell data stream post-processor. If accurate, the computed solution should have represented zero forces and zero moments for all axes, other than the constant force in the negative z-direction. Any other non-zero values would be erroneous. The hanging mass was chosen to be 12.2Kg, a value providing roughly 20% of full scale for the $M_x$ and $M_y$ moment channels, and 10% of full scale for the $F_x$ and $F_y$ force

channels. This was the largest mass that fit within the spatial constraints of the hip simulator.

### 2.4.2 Load Cell Post-Processing and Data Stream Analysis

### Validation: Experiment Results

A 5-second stream of the forces and moments measured by the load cell during the validation experiment is shown below.
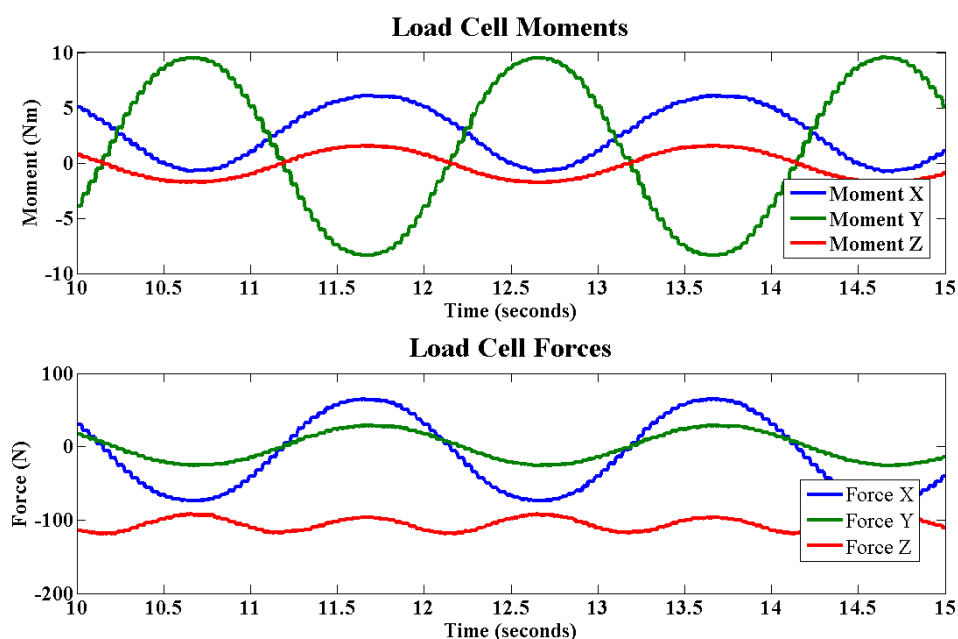


Figure 29. Plot of the data stream input to the post-processor. The moments (top) and forces (bottom) are with respect to the load cell during the test. It is apparent that all six channels of the six DOF load cell are active during the test.

The input data stream represents the un-modified values measured by the load cell during the test. Because the load cell had been previously calibrated, the accuracy of the input could be assumed. The input data were first transformed to convert from the coordinate system of the load cell to a coordinate system that had its origin coincident with the COR of the hip simulator. This new coordinate system was parallel with the load

cell, and was analogous to the coordinate system of the pelvis in described in Section 1.6.2.4. This transformation could be represented by a simple uniaxial translation from the load cell to the hip simulator's center of rotation. Both reference frames oscillated together throughout the test. The forces and moments with respect to this new coordinates system are shown in Figure 30.
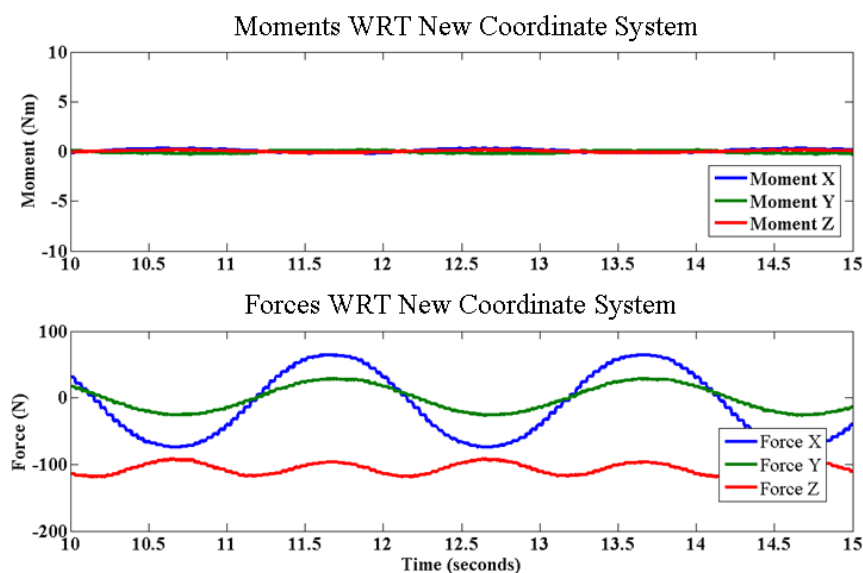


Figure 30. Plot of the forces and moments with respect to the moving coordinate system. Because the origin of the coordinate system was coincident with the center of rotation of the hip simulator, the zero-valued moments and non-zero valued oscillating forces indicated correct performance.

The moments with respect to the hip simulator's center of rotation were zero, while the forces continued to oscillate as expected. The final transformation of the forces and moments did not change the origin of the coordinate system, but instead transformed it from a moving coordinate system to a fixed coordinate system. The results of the final transformation are shown in Figure 31.
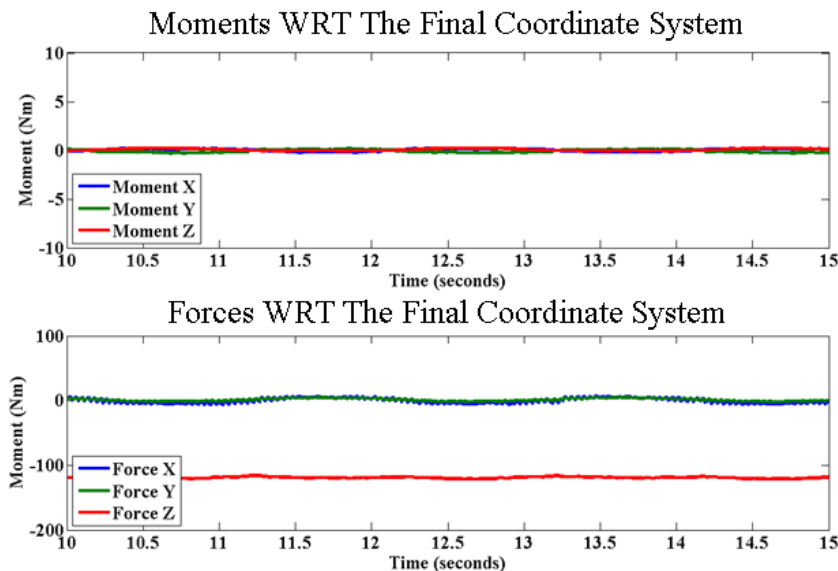
Figure 31. Graphs showing the moments (above) and forces (below) of a hanging mass with respect to a fixed coordinate system where the origin is coincident with the hip simulator's center of rotation.

All moments were zero, Fx and Fy were zero, and there was a force in the negative-z direction equal to the weight of the hanging mass (120N). The small fluctuations seen in the Fx and Fy forces were synchronous with the 0.4Hz hip simulator motions, and had an amplitude of 8N. The final transformation therefore represents a valid and expected result, confirming that the load cell data stream post-processing algorithm was accurate.

The 8N cyclic load was likely due to the swaying of the mass during the test. A swaying amplitude of less than 4 degrees would have been enough to create an oscillating force in a lateral direction equal to 8N. Swinging of approximately this magnitude was visually observed while the test was proceeding, although no steps were taken to quantify the magnitude of sway.

This (low) 8N sinusoidal error represented a very small percentage of the load cell's full scale range, and indeed was close to the resolution limit of the load cell. Thus,

the load cell data stream post-processor was proven to be accurate, with a acceptable level of error.

### 2.4.3 Joint Center of Rotation: Validation Experiment

To ensure that the method of determining the hip JC provided the desired accuracy, an experiment was designed to quantify the error involved. The testing setup consisted of a perfect ball joint with two joint members, representing a fixed member ('pelvis') and a rotatable member ('femur'). One marker was rigidly fixed to the (static) base of the ball joint, while three markers were placed on the (moving) 'femur'. While data were recorded, the 'femur' was moved throughout its range of motion, generating a cloud of 3D data points that were later used to resolve the JC. A static marker of known position was used to place the resolved JC within the reference frame of the base. To keep the experiment as relevant as possible, the 'femur' was moved with a similar range of motion as that of actual cadaveric specimens.

The HAAS mill was used to mill the joint's concave hemisphere in the base, as well as the fitted position for the fixed marker on the base. The hemisphere center and fixed marker were placed 25.4mm horizontally and 25.4mm vertically from each other, with no difference in height, to an accuracy of ±0.0254mm. The same method of data collection used in the actual experiment was used for this validation experiment. 3D coordinate data of all four makers were recorded at a rate of 100Hz for 45 seconds. This capture was then repeated three more times to create a suitable sample size.

The total error in determining the JC was comprised of two distinct error sources. The measurement error was from the Qualisys motion capture system, and the second error was from the computational technique that determined the JC from the Qualisys data. Ideally, no error would be introduced in the computational stage. An experiment was derived to quantify the amount of error added.

Measurement error was defined as the standard deviation of the fixed marker's 3D coordinates over the duration of the test. Precedent for use of position data standard deviation to quantify error was taken from the work of Comomilla et al.,[61] who used this as a metric to compare different functional methods for determining the hip JC. Total error (solution error) was defined as the difference between the computed and true center of rotation. The error introduced by the computational method (computation error) was equal to the difference between the solution error and the measurement error.

For the JC determination to be considered accurate, the solution error needed to be less than 1.41 times the measurement error, as described mathematically in Equation 6. This error constraint assumes that the propagation of error is additive and that the computational error is less than or equal to the measurement error. In addition to the limits set for the computational error, the final solution needed to have an average per-axis error less than 1mm. This 1mm distance error for each axis was the spatial resolution afforded by the graduated reference guides used for placing the specimen within the hip simulator. An error smaller than 1mm in solving for the JC would be overwhelmed by error inherent in simply placing the specimen within he hip simulator.

Equation 6. Verification that if computational error is less than the measurement error, then the solution error should be less than 1.41 times the measurement error.

$$\sigma_s = \sqrt{\sigma_m^2 + \sigma_c^2}$$

**If**     $\sigma_s$ = Solution Error

$\sigma_c \leq \sigma_m$     $\sigma_c$ = Computational Error

**Then**     $\sigma_m$ = Measurement Error

$\sigma_s \leq \sqrt{2} * \sigma_m$

2.4.4 JC of Rotation Validation: Experiment Results

The measurement error and solution error comparisons were expressed per-axis, as well as an average for all three axes. The results expressed graphically were:
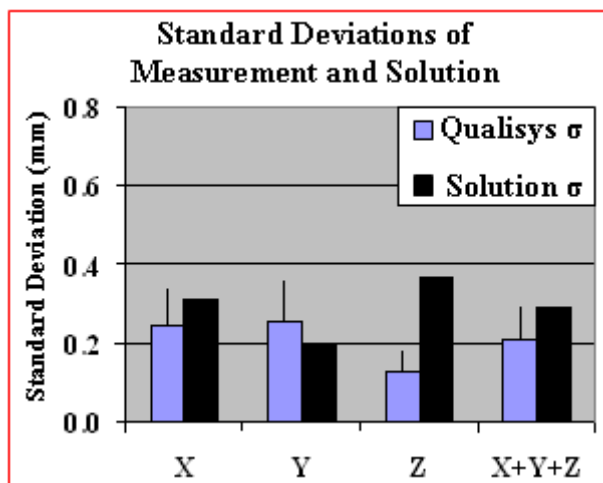


Figure 32. Graph of the measurement and solution error per-axis, as well as the average for all three axes. The dispersion bars on the Qualisys bars have a height equal to 0.41 times that of the bar height. Thus, a Qualisys bar and its respective dispersion bar have a combined height equal to the 1.41 error constraint.

The data presented in Figure 32 show that the solution error was less than 1.41 times the measurement error for the x- and y-axes, and for the average of the x-, y-, z-axes. This result confirmed that for those two axes and for the average, the error introduced in the computation step was equal to or less than the measurement error. The solution error for the z-axis was greater than the 1.41 times measurement error. It should be noted that the z-axis average absolute error of solution (Figure 33) was considerably lower than the other axis. This suggests that the goal of producing a solution error less than 1.41 times the z-axis measurement error was more exacting for the z-axis than for either the x- or y-axis due to the low magnitude of the z-axis.

The second criterion for evaluating the accuracy of solving for the JC compared the explicitly solved center to the true known center. The difference between the two was considered the total solution error. The error is expressed in mm for each individual axis in addition to the average error of all three axes. The results are shown in Figure 33.
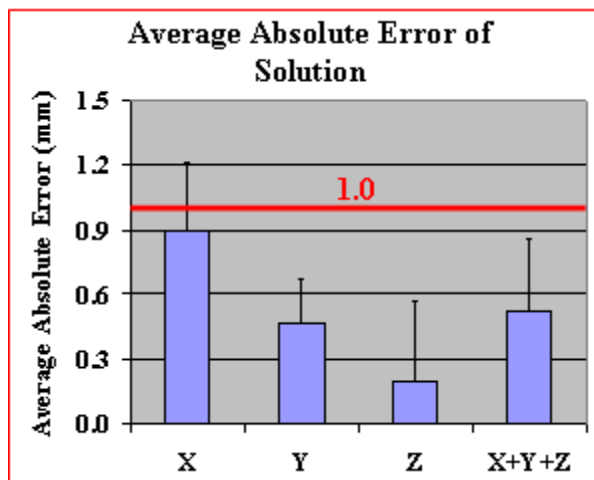


Figure 33. Average absolute error of the computed solution for each individual axis, and for the average of the three axes. The bold horizontal red line represents the predefined 1mm maximum allowable error limit.

Figure 33 confirms that the computed rotational center solution was on average less than 1mm from the true location of the center of rotation. The average absolute error for the x-axis was near this limit while the y-, z-, and average of the three axes were considerably lower. This result confirmed that the method for determining the JC had an acceptable level of error

Published results have documented that the accuracy of a computed rotational center solution is proportional to the range of motion utilized for data collection.[68] This consideration was taken into account in choosing the range of motion used during the validation test. The range of motion was similar to that which was used with cadaveric specimens (Figure 34). The arc angles between each pair of 3D data points were

calculated, and the maximum arc angle for a given data set was taken to represent the data set's range of motion. The range of motion for the validation was calculated to be 58.4°, slightly lesser than a cadaveric specimen's range of motion (Specimen 1 used in the sit-to-stand kinematic challenge), which was 58.7°.
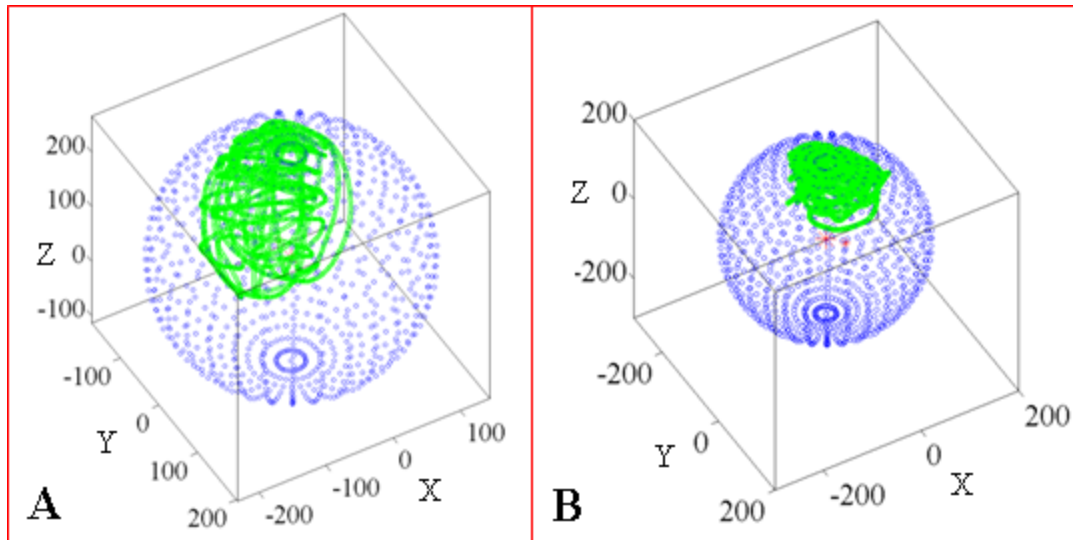


Figure 34. Side-by-side comparison of the range of motions used in determining the joint center of rotation for a cadaveric specimen (A) and surrogate hip (B).

# CHAPTER III: MATERIALS AND METHODS FOR IMPINGEMENT/DISLOCATION EXPERIMENTS

This chapter outlines the materials and methods used in testing cadaveric hemi-pelves in the hip simulator. The steps taken in preparing the fresh-frozen cadaveric tissue for testing are discussed, as well as how each specimen was cleaned and modified, how the specimen was oriented and potted in PMMA, and how the 3D position data were acquired for determining the JC. Subsequently, two distinct experimental procedures used for testing cadaveric specimens with the hip simulator are presented.

## 3.1 Cadaveric Specimen Preparation

The main steps in tissue preparation included specimen cleaning and soft tissue removal, reference frame orientation and potting within PMMA, JC determination, and finally specimen placement within the hip simulator.

The method of cadaveric specimen preparation was designed to produce a mounting surface on the specimen that mated with the interface provided by the updated hip simulator. Necessary to this end was establishing a specific spatial orientation that allowed for consistency between specimens, and for precise determination of the JC. The latter requirement was paramount in preventing erroneous load and moment data, resulting from malalignment between the JC of the specimen and the COR of the simulator.

### 3.1.1 Specimen Cleaning and Tissue Removal

The first step in preparing the specimen was removing excess soft tissue from the bony substrate of the pelvis and femur. Care was taken to preserve the hip capsule and all of its insertion sites. Initial specimen preparation included separating the hemi-pelves at the symphysis pubis and sacroiliac joint (Figure 35) using an osteotome and scalpel.
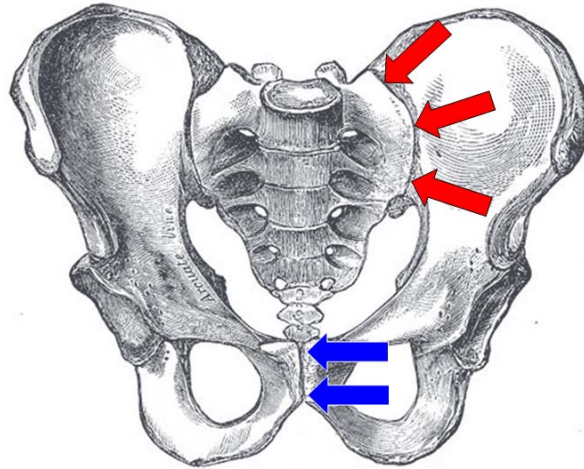
Figure 35. Drawing demonstrating the sacroiliac joint (red arrows) and symphysis pubis (blue arrows) of the pelvis. Both are separated during specimen preparation to produce two hemi-pelves.

The femur was then cut distally approximately 15cm from the greater trochanter, using a coarse-tooth hack saw (18 teeth per inch). This is demonstrated in Figure 36. Next, the pelvis was cut so as to create a superior facet parallel to the specimen's anatomical horizontal plane. This was done by first palpating the anterior superior iliac spine (ASIS), followed by the anterior aspect of the pubis. These two points and the symphyseal surface were used to define the vertical plane. The symphyseal surface (parallel to the saggital plane) was used to define an orthogonal surface that intersected both of these palpated points. This second plane was equivalent to the vertical plane. With both the vertical and saggital planes thus defined, the anatomical horizontal plane could be determined. The cutting line was drawn in the horizontal plane, intersecting the ASIS (Figure 36). The distance from the newly cut surface and joint center ensured that sufficient bone surfaces were available for PMMA-bone adhesion. Once cut, 4mm diameter, 38mm long, self-drilling screws were inserted into the pelvis to improve its potting anchorage strength. The screws were set normal to the pelvis' surface, in a row parallel to the newly cut surface. They were spaced evenly from each other, and roughly

15mm from the cut surface. In a similar manner, screws of the same diameter, albeit shorter, were added to the femur.
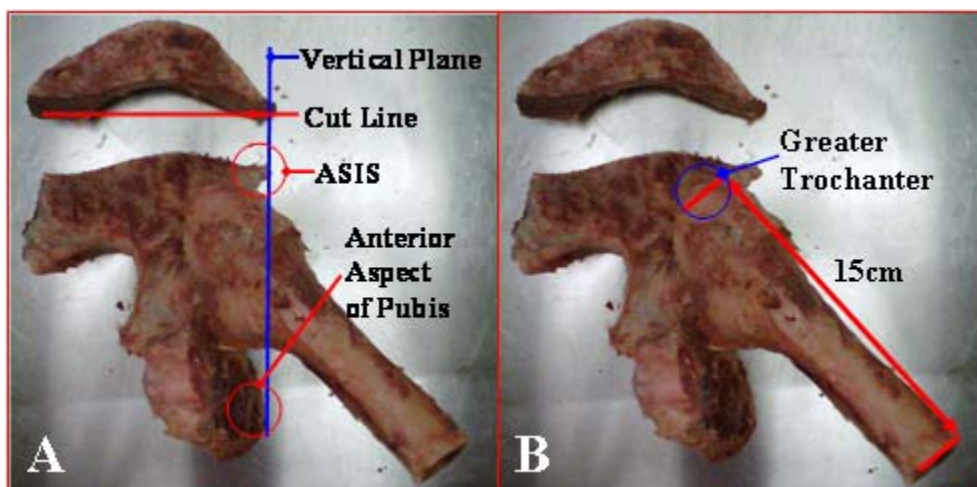


Figure 36. Photographs showing the palpation points and reference lines used in trimming a right hemi-pelvis (A), and those used in determining the length of the femur (B).

### 3.1.2 Specimen Orientation and Potting in PMMA

Once the specimen had been properly cleaned and incised, the hemi-pelvis was potted in dental-grade PMMA. The hemi-pelvis was placed upside-down within the potting box, so that the specimen's anatomical horizontal plane was aligned with the x-y plane of the potting box. The symphysis pubis was used to define the upright orientation of the specimen. The specimen was oriented so that this surface was normal to the potting box's x-z plane. To stabilize the pelvis while the PMMA cured, a support arm rigidly fixed to the potting box was attached to the ramus of the ischium (Figure 37). The potting box was then filled with approximately 0.35 liter of PMMA, mixed from 160g of powder and 80g of liquid methyl methacrylate monomer.
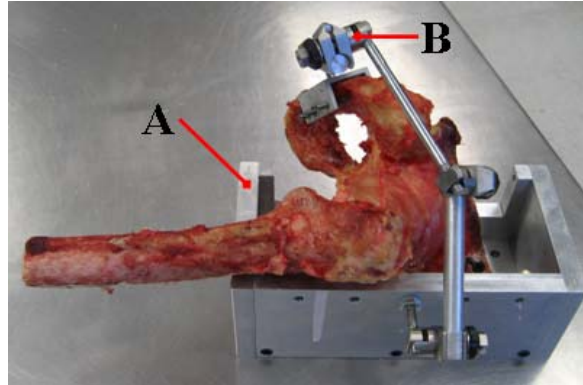
Figure 37. Photograph of the specimen just prior to being potted with PMMA. The potting box (A) determined the shape of the mold, and the support arm (B) held the specimen in place while the PMMA cured.

The femur was potted in its corresponding box after the hemi-pelvis PMMA had cured and had been removed from its mold. Approximately 0.15 liter of PMMA was mixed in the same 2:1 dry-to-liquid proportion noted above, and was cast to form a regular cylinder.

### 3.1.3 Joint Center Determination and Specimen Placement
### within the Simulator

To find the JC, the above described iterative method was used to minimize a geometric cost function. The data used for this purpose were provided by an optical motion capture system. Again, the system used was a 3-camera system made by Qualysis© of Sweden (Figure 38).

Figure 38. Photograph of the Qualysis 3-camera system used to collect 3-D position data for resolving the specimen's JC.

3D position data were collected from four 3mm diameter reflective markers. Three markers were placed upon the femur along its long axis, and one marker was placed at a known position with respect to the pelvis' rectilinear PMMA base (Figure 39-a).
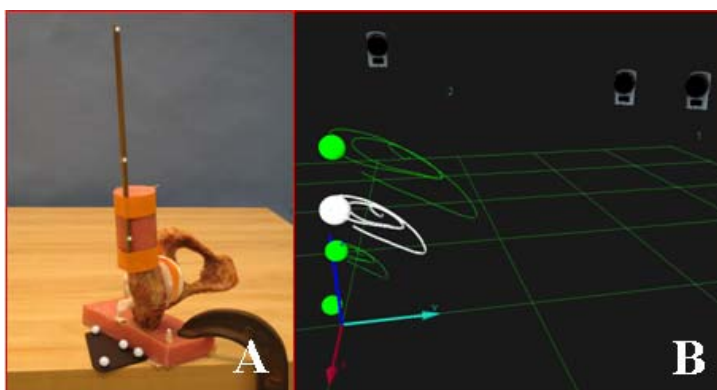


Figure 39. Photograph of the specimen with optical markers (A), and a rendering of the resulting cloud of data points recorded during motion capture (B).

During data capture, the pelvis was held fixed in space while the femur was moved throughout its range of motion. Care was taken to prevent joint impingement. Data capture occurred for 45 seconds at 100Hz, providing 4500 cartesian coordinates for

each marker (Figure 39-b). The data file output from Qualysis© software was then input to a custom analysis program written in MATLAB. This program's output provided the user with the basis for specimen placement within the hip simulator, in the form of x, y, and z coordinates that were with respect to the specimen's PMMA block. These coordinates were aligned according to graduated reference markings on the simulator mounting. This achieved concentricity between the specimen and hip simulator.

<div align="center">

3.2 Effect of Rigid Posterior Capsule Attachment During

Hip Flexion

</div>

Investigating the change in resisting moment during a 0º to 90º flexion was first undertaken, to verify high resisting moments (20Nm) computed by a preliminary FE solution. By physically testing a cadaveric pelvis, and incrementally reducing hip capsule laxity, it was thought that the testing variant that best matched the computed results would provide insight as to how to adjust the FE model.

In this section, the methods for experimentally determining the effects of surgically inducing rigid posterior capsule attachment during a simple hip flexion are described. A fresh-frozen hemi-pelvis was prepared, and placed within the hip simulator in accordance with the above-described protocols. Flexion from 0º to 90º was delivered at a rate of 9º per second, while a 300N compressive axial load was applied to the specimen.

Overly tight posterior capsule bone attachment was first created by screwing 4 size-6 sheet metal screws posteriorly and circumferentially into the neck of the femur (Figure 40).

Figure 40. A right cadaveric hip, viewed from posterior-superiorly. The four screws used to achieve rigid fixation of the posterior capsule are visible.

The posterior portion of the capsule was then sutured to the screws, while the joint was at either 0º or 45º flexion (to represent different definitions of the 'capsule-neutral' joint flexion angle), thereby reproducing the conditions of posterior capsule attachment modeled in the FE analysis.

The pelvis was first tested before the aforementioned capsule fixation procedure was done, to provide an experimental baseline. The hip was then tested with the screws, but without sutures. In the two subsequent testing sequences, the capsule was sutured while the joint was at 45º and then at 0º of flexion, simulating rigid posterior capsule attachment with capsule-neutral distention at 45º and 0º, respectively. A final three test sequences examined the effects of incremental damage of the hip capsule, simulated by varying degrees of posterior acetabular detachment. The results of these trials were used in validating computed regional detachment from the capsule's acetabular insertions. Regional capsule detachment was simulated with three experimental configurations. In the first configuration, approximately 3/8ths of the capsule was incised posteriorly, near the acetabulum. In the second configuration, approximately half of the capsule was incised posteriorly near the acetabulum. In the third and final configuration, the entire

capsule was incised near the acetabulum. Each of the seven tests were repeated four times, necessarily conducted in the order described.

### 3.3 Sit-to-Stand Experimental Testing Procedure

The primary goal of the sit-to-stand experiment was to provide *in vitro* evidence that could be used in validating the hip capsule FE model. To provide the most direct correspondence between FE analysis and *in vitro* experimentation, the experimental input conditions were based on pre-existing, successfully completed FE analyses. Doing so guaranteed that direct comparisons could be made between the two. Although there were many hip joint kinematic challenges that had been modeled computationally, only a subset could be reproduced with the hip simulator. Joint ROM was somewhat limited by kinematic constraints of the hip simulator, and structural components (especially the load cell) had load limits that restricted the magnitude of axial load that could be applied to the specimen. Axial joint forces used in the FE model to simulate physiological dislocation were nearly an order of magnitude greater than the load cell's limits, so for the experiment these loads needed to be reduced to safe levels. From the set of available kinematic challenges, a sit-to-stand maneuver was adapted for use in the hip simulator.

A transpelvic implantation procedure was performed after the cadaveric specimen had been prepared. The transpelvic implantation procedure allowed placement of "THA" components within the specimen, while fully preserving the structural integrity of the hip capsule. This procedural advancement specifically allowed evaluation of the mechanical contribution that the joint capsule had on dislocation events of a THA-implanted hip. This ability to test a prosthetic hip with an intact capsule allowed the specimen to closely replicate the fully-healed-capsule configuration modeled by FE analysis. An additional feature of the transpelvic procedure was that the anteversion and tilt of the poly liner was adjustable, thus allowing study of a variety of surgically plausible cup orientations. For the three specimens that were tested, three orientations were examined per specimen.

Each set of orientations included a neutral poly-liner orientation that imitated the orientation of the anatomic acetabulum of the specimen. The orientations are portrayed in the Table 1, below.

Table 1. Table of poly-liner orientations.

| Specimen | Liner Orientation | Tilt | Anteversion |
|---|---|---|---|
| Specimen #1 | 22.7°T 30°A | 22.7° | 30° |
| | 57.3°T 10°A | 57.3° | 10° |
| | Neutral | 40° | 20° |
| Specimen #2 | 20°T 20°A | 20° | 20° |
| | 40°T 0°A | 40° | 0° |
| | Neutral | 40° | 20° |
| Specimen #3 | 22.7°T 30°A | 22.7° | 30° |
| | 57.3°T 10°A | 57.3° | 10° |
| | Neutral | 40° | 20° |

The cup orientations were modified after Specimen #1, due to a continually evolving testing procedure. The orientations used in the experiments involving Specimen #2 were thought to provide greater distinctions between their impingement events.

The sit-to-stand kinematic challenge was a truncated version of the challenge used in the FE analysis. This was done in part to avoid portions of the movements that could not be replicated due to physical limits of the hip simulator, and in part to reduce the testing time. The steps of the kinematic challenge are reported in Table 2. Each step was completed in two seconds, with the entire challenge lasting 6 seconds.

Table 2. Sit-to-stand kinematic challenge steps.

| Step | Adduction | Flexion | Internal Rotation |
|---|---|---|---|
| Starting Position | 0° | 60° | 0° |
| 1 | 2° | 94° | 2° |
| 2 | 13.3° | 104.3° | 1.4° |
| 3 | 14.3° | 105° | 2.3° |

### 3.4 Transpelvic Implantation Procedure

The transpelvic procedure is a unique experimental protocol for surgically placing THA hardware within a specimen, without violating the hip capsule. The transpelvic procedure allowed for the testing of specimens that were essentially identical to those that were modeled in the FE analysis. In the transpelvic approach, the acetabular component is inserted through a hole created on the inside surface of the pelvis, aligned with the acetabular rim and with the hip joint center. The femoral component (Figure 41) is inserted through the long axis of the femoral neck, unlike a traditional femoral component, which is placed within the medullary cavity. A CAD drawing of the femoral component is shown below.
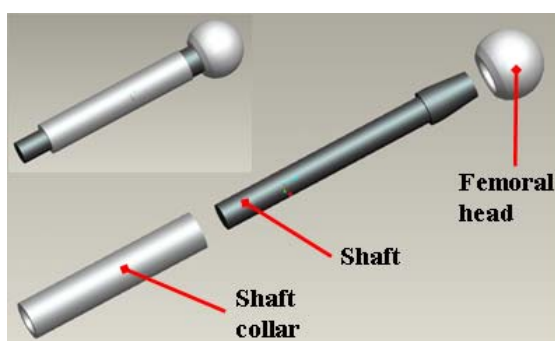


Figure 41. CAD drawing of the femoral component used in the transpelvic procedure.

The shaft collar is rigidly attached to the femur with PMMA, and the shaft and femoral head construct remain seated in the shaft collar due to a constant compressive force applied during testing. The femoral head was produced by DePuy, and had a diameter of 28mm, while the shaft collar and shaft were machined in-house from aluminum. Spacers placed between the shaft and shaft collar were used to vary the effective neck length. This feature allowed avoiding mal-placement of the femoral component due to over- or under-recovering the neck length, and it allowed for correction for initial placement errors.

The procedure began with a specimen that had been prepared by first removing all soft tissues from the hemi-pelvis, except of course for the hip capsule. The length of the femur was trimmed to approximately 15cm, measured from the greater trochanter to the most inferior point. The femur was then potted in PMMA, within a cylinder approximately 10cm in length and 5cm in diameter.

An experienced orthopaedic surgeon performed the transpelvic implantation procedure for every specimen. The procedure began by positioning the joint so that the long axis of the femoral neck was normal to the plane coincident with the rim of the acetabulum. In this position, a 1.6 mm diameter Kirschner-wire (K-wire) was drilled through the long axis of the femoral neck and through the hemi-pelvis (Figure 42). This K-wire acted as a guide for THA component placement. The placement was first estimated, and then checked visually using a single coronal x-ray (Figure 43).
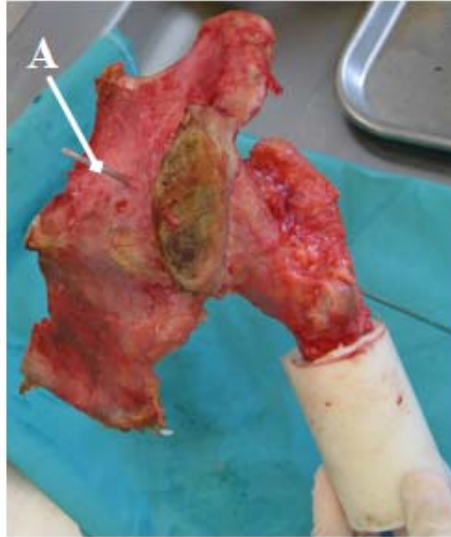
Figure 42. Photograph of the medial side of the hemi-pelvis specimen. The K wire (A) is shown protruding from the pelvis, having entered through the femur along the neck.
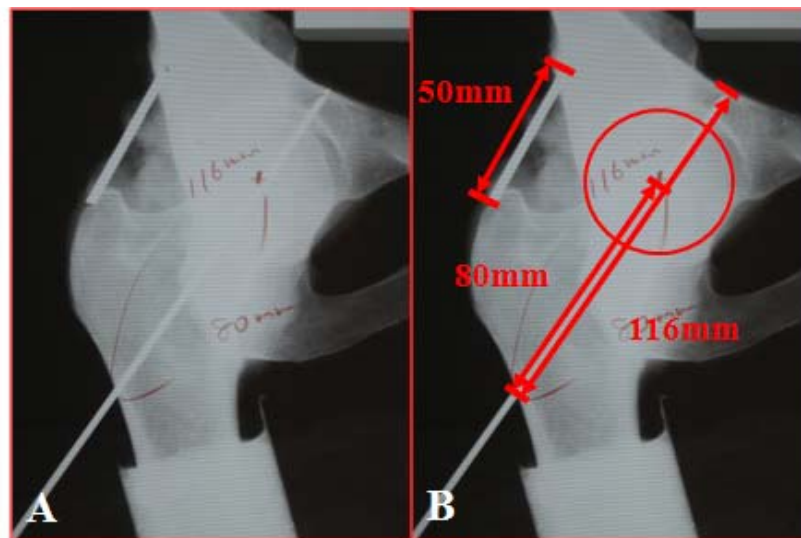


Figure 43. X-ray of the hemi-pelvis (A). The annotated radiograph (B) reveals that the K wire was indeed appropriately placed, and shows measurements of the effective neck length and distance between joint members.

From the radiograph, the orientation of the K-wire could be checked, and used for re-positioned if necessary. Additionally, a measurement analogous to effective neck length was made with respect to bony landmarks along the K-wire. From the radiograph,

the measurements taken were used to determine implant component placement. The neck of the femoral component could be extended to increase neck length, and the liner could be adjusted along its axis to adjust the joint's center of rotation. Using Figure 43-b as an example, the specimen's implanted components needed to be placed so that the distance between the peritoneal surface and lateral surface of the femur (measured along the K-wire) remained at 116mm, and the distance between the JC and lateral surface of the femur stayed at 80mm.

Next, the medial surface of the hemi-pelvis was prepared for the attachment of the peritoneal-side collar (Figure 44). Bone protrusions were removed using an oscillating saw, thereby producing an approximately flat surface for attachment.
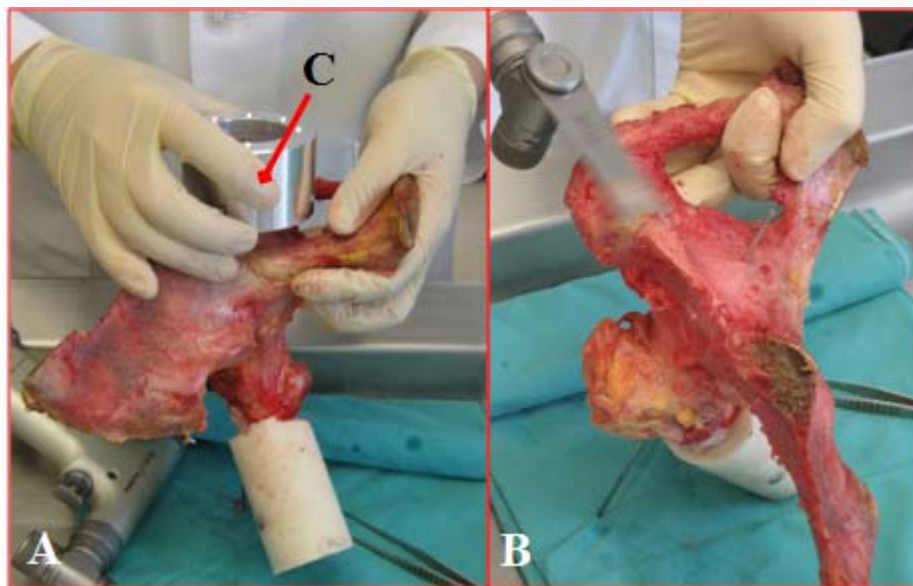


Figure 44. Photographs of experimenter determining the placement of the pelvis-side collar (A), and subsequently creating a flat mating surface with an oscillating saw.

Once a suitable surface had been prepared, the pelvis-side collar was secured to the specimen with 76mm long size-6 self-drilling screws. The number of screws varied

by specimen and available surface area. Alignment of the peritoneal-side collar was determined using the aforementioned K-wire and drill guide. The secured collar is illustrated in Figure 45.
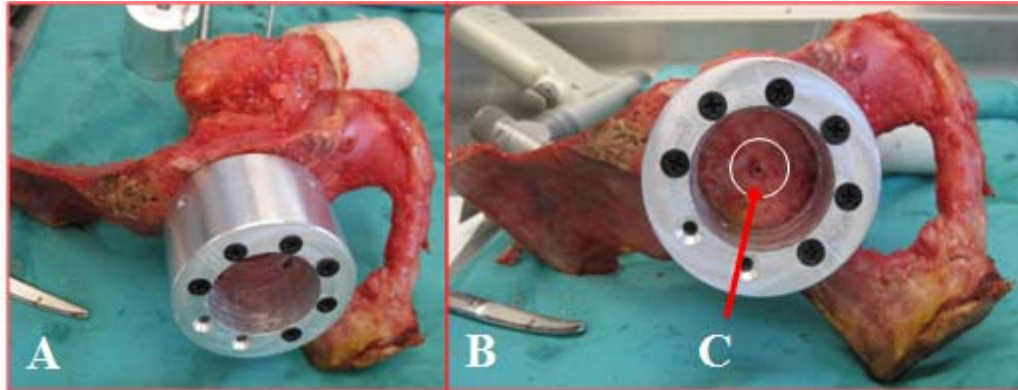


Figure 45. Photographs (A,B) of an attached peritoneal-side collar. The hole (C) created by the K-wire is shown at right.

In addition to guiding the hole saw that was used for removing interstitial material from the pelvis, the pelvis-side collar served to support the specimen. Figure 46 shows the specimen in its stand with the hemi-pelvis being cut with a hole saw.
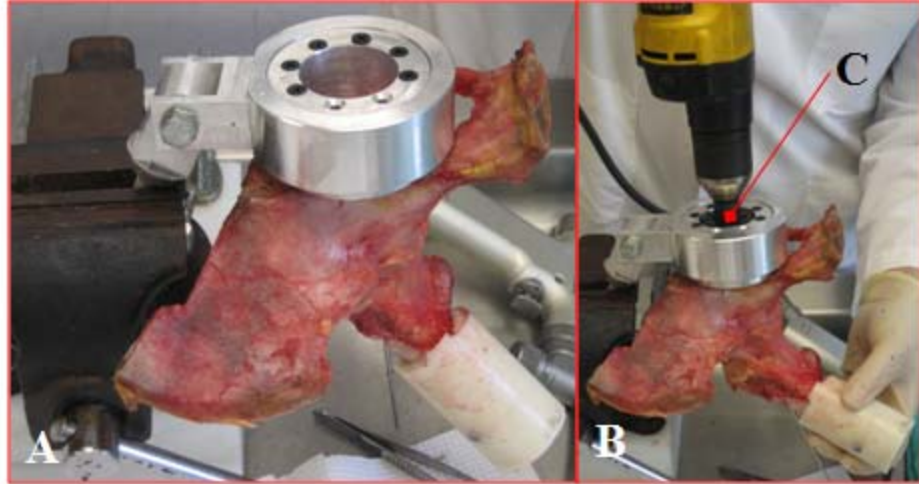
Figure 46. Photographs showing the specimen in its support (A) and while being cut (B)
with the hole saw (C).

Once the pelvis was cut, access was gained to the joint space through the
peritoneal-side collar. The hole for the femoral shaft-collar was made using progressively
larger reamers, to increase the diameter of the hole until it was at the desired dimension.
This process is depicted in Figure 47. With the K-wire inserted into its initial position
along the long axis of the femoral neck, a K-wire-guided reamer was used to enlarge the
hole to a diameter accessible by a second reamer. From this initial 13mm hole, two
additional reamers extended the diameter to 14mm and then 15mm.
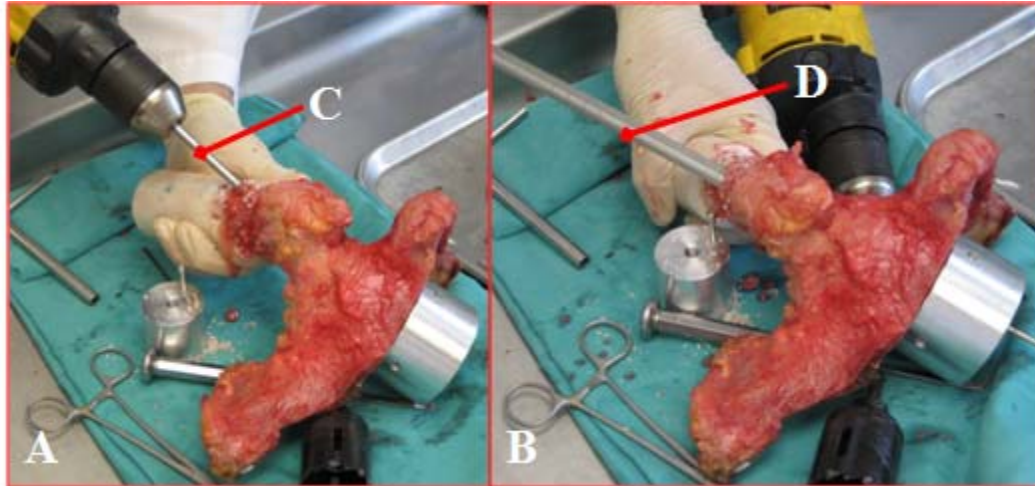
Figure 47. Photographs depicting enlargement of the hole for the femoral THA
component. The left photograph, A, shows the initial drilling with the k-wire
guided reamer (C). The right photograph, B, shows the use of a 16mm reamer
(D).

Through the peritoneal-side collar and the just-created 41.275mm hole in the
pelvic wall, the femoral head was ablated from the femur, using both an oscillating saw
and manual fragment extraction (Figure 48). To avoid hip capsule damage from soft
tissue impingement during testing, care was taken to remove all sharp edges that had
been created when the femoral head was removed. If this were not done, there would be a
possibility that the hip capsule could be torn during impingement.
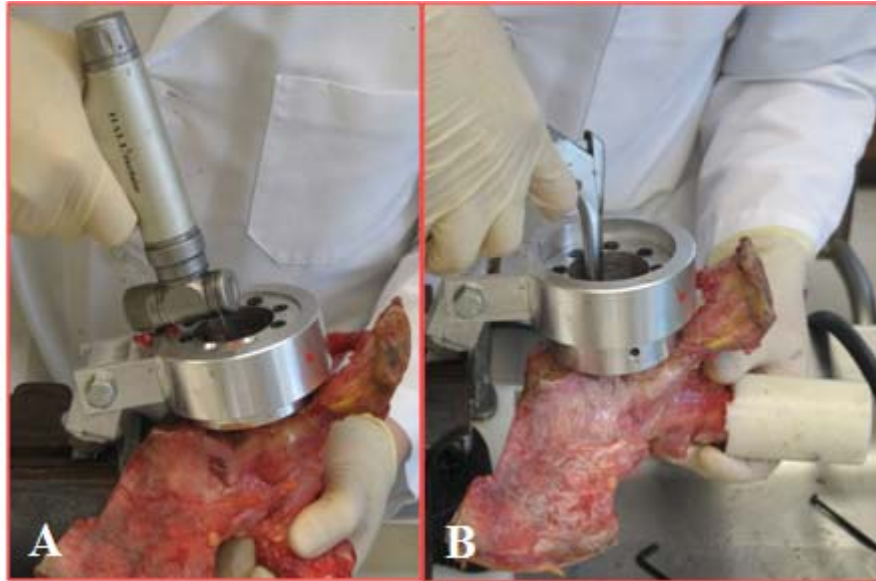
Figure 48. Photographs showing the use of an oscillating saw to remove the head of the femur (A), and the experimenter manually removing bone fragments (B).

Once all unnecessary bone had been removed from the femur, the femoral shaft-collar was inserted into the 15mm hole through the femoral neck. Using measurements of the THA hardware, and those from the initial radiograph, the shaft collar was then placed and fixed using PMMA (Figure 49).
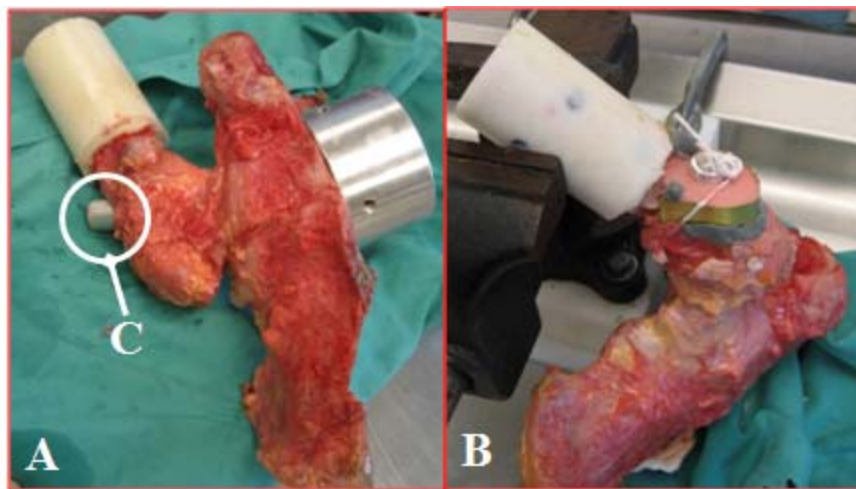


Figure 49. Photograph showing the insertion of the shaft-collar (C) in the femur (A), and the securing of the shaft-collar with PMMA (B).

PMMA fixation was augmented by two screws inserted into the femur near the greater trochanter. Once the PMMA had cured, the aluminum-backed poly liner was inserted into the peritoneal-side collar. Using the previously taken radiograph and the known dimensions of the acetabular component, the depth and rotation of the aluminum-backed poly liner were set.

Component placement was checked with a final radiograph of the joint in the coronal plane (Figure 50). Joint space could be altered by either changing the depth of the acetabular component, or by adding spacers between the femoral shaft and shaft collar. Using the radiograph in Figure 50 as an example, the space between the femoral shaft and shaft-collar needed to be reduced by 4mm (4mm = 84mm – 80mm), and the depth of the acetabular component needed to be deceased (i.e., moved medially) 2mm (2mm = (84mm- 80mm) – (118mm – 116mm)).
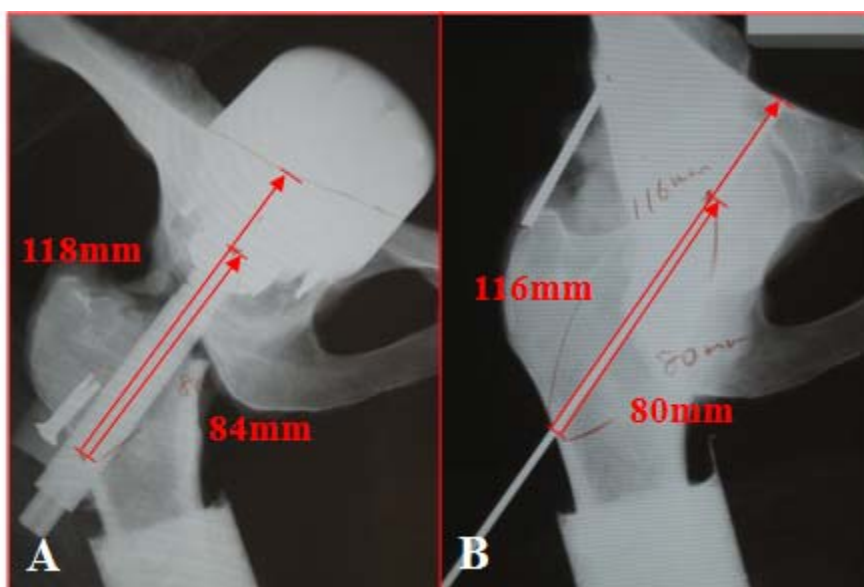


Figure 50. Radiographs showing the placement of the THA components, with the native joint used as a reference.

CHAPTER IV: RESULTS

In this chapter, the results for experiments described in Chapter 3 are presented, both for the effect of rigid posterior capsule attachment during hip flexion, and for the kinematic sit-to-stand challenge.

### 4.1 Effect of Rigid Posterior Capsule Attachment During
### Hip Flexion

An intact capsule served as a control for the experiment. It was hypothesized that artificially removing the laxity in the posterior segment of the hip capsule would increase the resisting moment during joint flexion, a phenomenon observed in the development phase of the FE model.

The results of the experiment are provided in Figure 51. The resisting moment is plotted with respect to joint flexion.
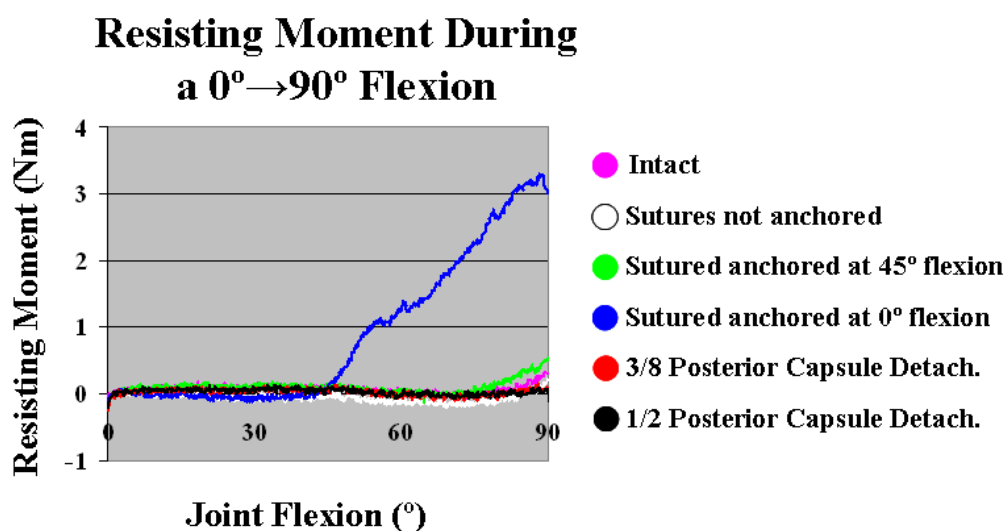


Figure 51. Resisting moment with respect to joint flexion for six different testing configurations. By far, the highest resisting moment occurred when the hip capsule was sutured at 0º flexion.

The data showed that the resisting moments developed during flexion were relatively similar in magnitude for the intact baseline, un-anchored configuration, and when the posterior capsule was sutured at 45º flexion. The configuration where a portion of the posterior capsule had been detached showed a slight decrease in resisting moment compared to the intact configuration. During the testing configuration where the posterior capsule had been sutured at 0º flexion, it was apparent that the capsule tore at approximate 85º of flexion. The drop in resisting moment while flexion was increased indicated that an unknown amount of structural integrity had been lost. A peak of 3.3Nm of resisting moment was measured in the first trial, while approximately only 2.3Nm was measured in the subsequent tests (Figure 52).
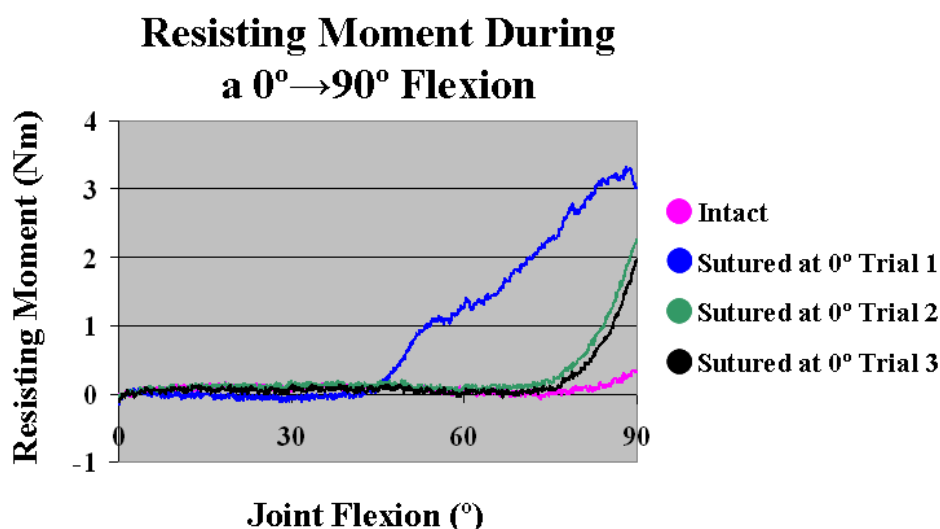


Figure 52. The resisting moments with respect to joint flexion are plotted for the three trials where the posterior portion of the hip capsule had been rigidly fixed at 0º flexion. The intact configuration is plotted for comparison.

The damage to the capsule that occurred in the first trial presumably affected the subsequent trials, whose peak moment was reduced by 30%. As this was the last testing

configuration before the posterior capsule detachments were simulated, the damage done to the capsule did not affect the results of the subsequent test configurations.

The trial in which the capsule was completely detached resulted in frank dislocation at the start of the test. No suitable results could be salvaged, and for this reason this sequence was excluded.

## 4.2 Sit-to-Stand Experimental Testing for a Cadaveric Specimen with THA components

The Sit-to-Stand kinematic challenge was performed with three cadaveric specimens having had hardware implanted in accordance with the previously described transpelvic implantation procedure. The capsules of the specimens were successfully preserved throughout the preparation process. During preparation of the first specimen, x-rays were not taken to determine joint parameters such as JC and distance between joint members. This procedural step of taking x-rays was not added until the second specimen. For this reason, only the second specimen has evidence directly confirming that the location of the JC and distance between joint members approximated those of the native joint.

In the first specimen, the experimental variable was the poly liner orientation during the joint motion simulation (see Table 1, page 63). It was hypothesized that the different orientations would result in disparate impingement events, indicated by different resisting moment magnitudes occurring at different amounts of flexion. 22.7ºT 30ºA, Neutral, and 57.3ºT 10ºA cup orientations were tested, and four replicate trials were performed per test. No observable damage to the hip capsule occurred during testing. Impingement occurred in all test cases (Figure 53).

**Resisting Moments for Three Cup
Orientations During Sit-to-Stand**
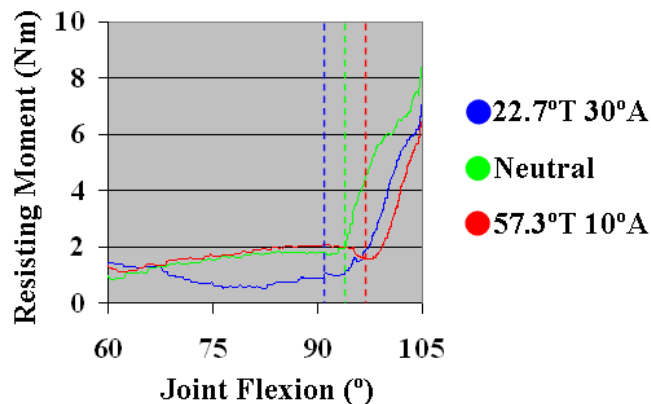


Figure 53. Graph of the resisting moment developed during a sit-to-stand kinematic
challenge. The dotted blue, green, and red lines indicate initial impingement
for the 22.7ºT 30ºA, neutral, and 57.3ºT 10ºA orientations, respectively. The
white lines designate points of kinematic discontinuity.

As expected, the 22.7ºT 30ºA poly liner orientation impinged first, followed by
the neutral, followed by the 57.3ºT 10ºA. Occurrence of the impingement event was
determined using the resisting moment magnitude curve, and transverse displacement of
the femur measured during testing. During impingement, the pelvis was constrained from
moving translationally, which instead forces the femur to move in the x-y plane during
subluxation or dislocation. Figure 54 illustrates how femur transverse motion was used to
indicate an impingement event. Both the anterior/posterior and medial/lateral
displacements exhibit no change during flexion from 60º to 70º. Then an abrupt
displacement is witnessed at 70º of flexion followed by a continual increase in
displacement. This increase in displacement coupled with an increase in resisting moment
indicates the point of impingement.

## Impingement During a Kinematic Simulations
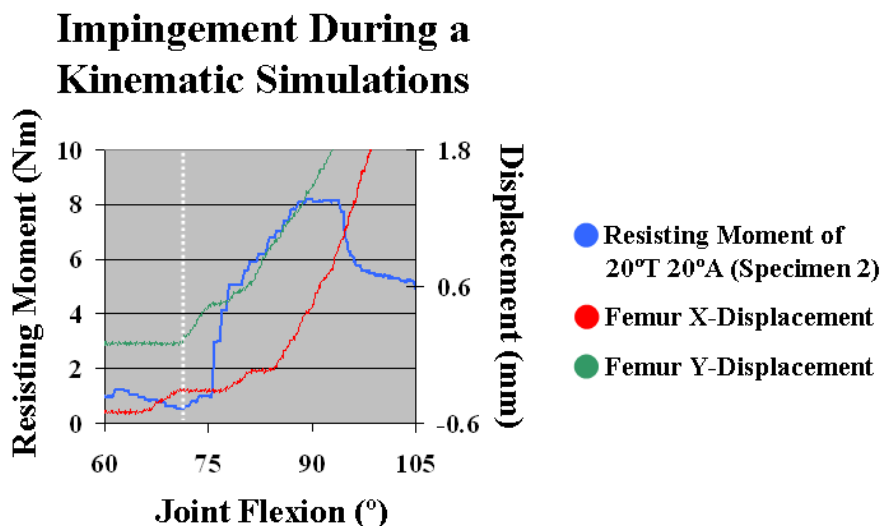


Figure 54. Graph illustrating how the event of impingement was determined. A discontinuity (white dotted line) in both the femur's x- and y-displacements (anterior-posterior and medial-lateral, respectively) followed by an increase in displacement combined with an increase in resisting moment are indicative of impingement.

The data indicate that the 22.7ºT 30ºA, neutral, and 57.3ºT 10ºA impinged at approximately 91º, 94.5º, and 97.5º of flexion, respectively.

During testing of the second specimen, the intactness of the hip capsule was evaluated along with cup orientation. The hip capsule was either fully intact, or was completely detached at the acetabulum. The cup orientations used were 20ºT 20ºA, 40ºT 0ºA, and neutral. The resisting moments that were developed during testing for the intact and completely detached capsule configurations are illustrated in Figure 55. Of the configurations where the capsule was completely detached, the resisting moment was entirely due to hardware impingement. The resisting moment of the intact capsule configurations was attributable to both the hip capsule stretching and hardware impingement. Impingement occurred at 72º, 94º, and 96º of flexion for the 20ºT 20ºA, 40ºT 0ºA, and neutral cup orientations, respectively.

Of the configurations with intact capsules, the resisting moment increased at approximately 75º of flexion. For the neutral and 40ºT 0ºA cup configurations the resisting moments prior to impingement were entirely due to capsule stretching. This 75º angle demarcating laxity and tension in the hip capsule corresponds to the resisting moment curve measured for an intact anatomic hip specimen during a 0º to 90º flexion (Figure 51). Figure 51 indicates that for an anatomic hip, resulting moment increase begins to occur at approximately 72º of flexion. For the natural and 40ºT 0ºA configurations, the resulting moment increase begins at nearly this same angle.
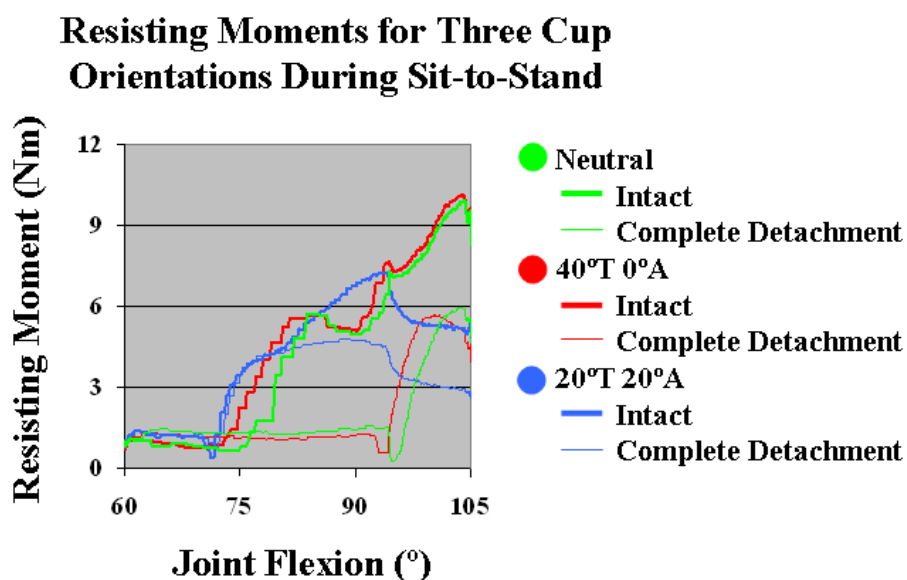


Figure 55. Graph comparing the resisting moments of three different cup orientations and two different capsule configurations during a sit-to-stand kinematic challenge. The resisting moment discontinuities that occurred for the completely detached capsule configurations are indicative of hardware impingement.

The third specimen was tested in a similar manner to Specimen 2. The intactness of the hip capsule was evaluated in addition to cup orientation. The hip capsule was either fully intact, or was completely detached at the acetabulum. Unlike Specimen 2, however, the three cup orientations that were tested with Specimen 3 were 22.7ºT 30ºA, neutral,

and 57.3ºT 10ºA. The resisting moments are graphed with respect to joint flexion in Figure 56. These were the same cup orientations tested with Specimen 1. The three cups impinged at flexions of 81º and 95.5º for the 22.7ºT 30ºA, neutral cups, respectively. The 57.3ºT 10ºA cup did not impinge during the experiment.
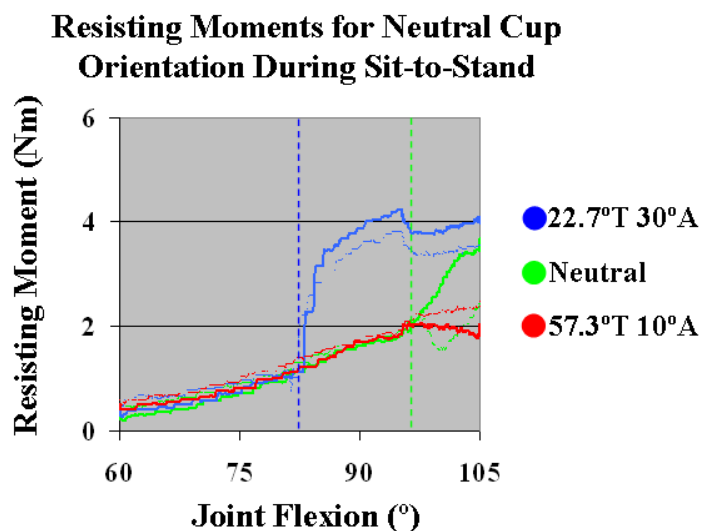


Figure 56. Graph comparing the resisting moments of three different cup orientations and two different capsule configurations during a sit-to-stand kinematic challenge. The dotted lines indicate the impingement event.

The resisting moments of the neutral cup orientations of Specimens 1, 2, and 3 are compared in Figure 57. For the specimens, impingement occurred at nearly the same flexion angle, separated by only 1.0 º. Despite this similarity, substantial rise in resisting moment for Specimens 1 and 3 did not occur until impingement.

**Resisting Moments for Neutral Cup
Orientation During Sit-to-Stand**
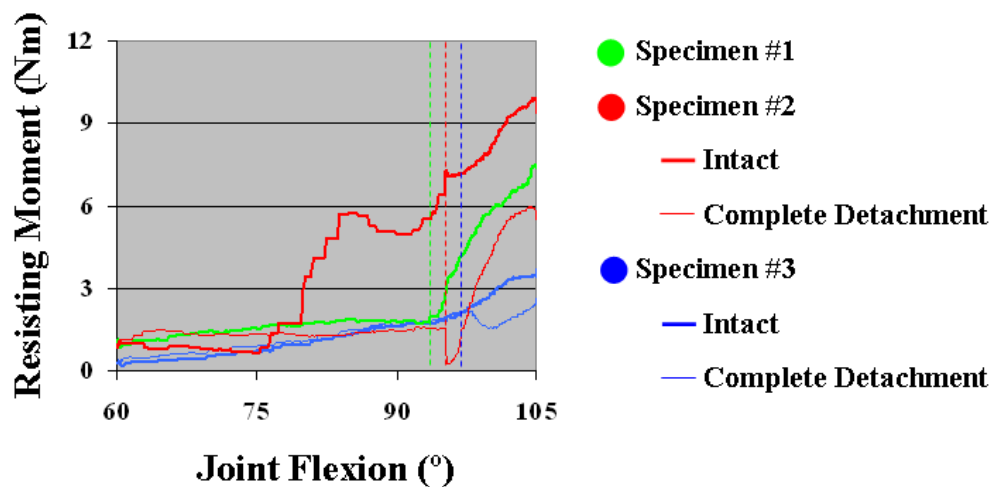


Figure 57. Graph comparing the resisting moments of Specimens 1, 2, and 3 when a neutral cup orientation was used. Impingement occurred at 94.5º, 95º, and 95.5º for Specimens 1, 2, and 3, respectively.

CHAPTER V: DISCUSSION

The proceeding sections discuss the results attained during the two cadaveric hip simulator experiments. Sources of error, areas where improvement is needed, and whether the research aims had been met will now be discussed.

### 5.1 Effect of Rigid Posterior Hip Capsule Attachment
### during Hip Flexion

The motivation for studying joint resisting moment during flexion grew from questions that had arisen regarding the moment solution from preliminary FE solutions. The FE model had suggested that the intact hip capsule was contributing large resisting moments (20Nm) at 90º of flexion. This called into question the constitutive formulation for the hip capsule, in that the posterior portion of the computational hip capsule apparently had less laxity than seen in native cadaveric hips.

The testing results support the paradigm that the posterior portion of the hip capsule is not tightly attached, but rather provides a significant level of laxity. This is evident by the stark difference in resisting moments of the native capsule versus the capsule sutured at 0º of flexion. The nominal resisting moment in the native capsule apparent during testing was as expected from handling the specimen before testing. The joint offered little perceivable resistance when it was manually flexed to approximately 90º, supporting the experimental finding that the capsule provides little resistance during flexion from 0º to 90º.

In initially processing the data, it was surmised that an error had occurred in physical placing the specimen within the hip simulator. Evidence for improper specimen placement was an artifactual resisting moment proportional to joint flexion superimposed onto the data. The original resisting moment curves are documented in Figure 58. In the figure, the resisting moment clearly increased in magnitude between 9 and 21seconds. During this time a 300N axial load was applied, with no joint motion. The rise in the

resisting moment is indicative of incorrect position, because if the joint center of the specimen had been aligned with that of the hip simulator, no moment would have occurred from an axial load, regardless of magnitude.
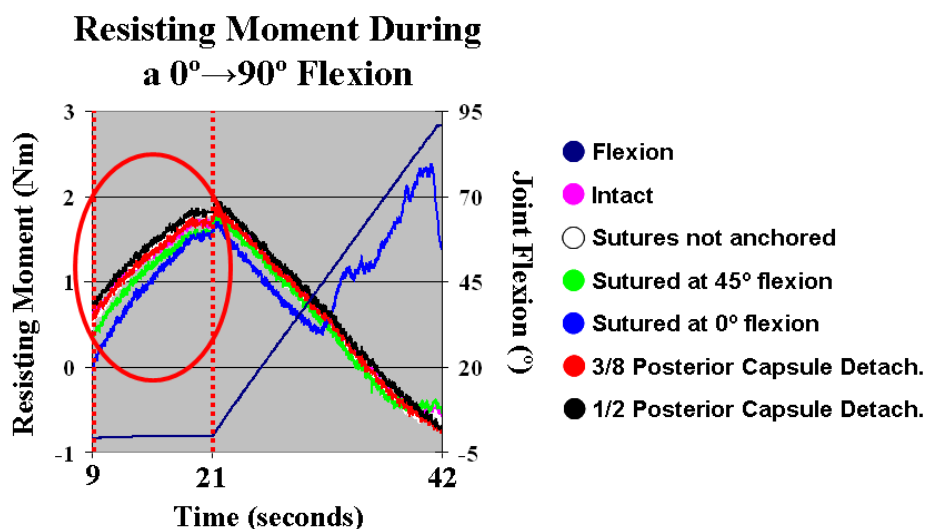


Figure 58. Figure indicating that the measured resisting moment of the specimen increased due to an increasing axial load while no change in flexion occurred. These moments are encircled in red. If the specimen had been placed perfectly (JC and hip simulator COR coincident), the slope would equal 0.

When the same data were plotted again, with joint flexion against resisting moment, a clear linear relationship can be seen between the two (Figure 59). The relationship was used to define a linear equation to mathematically remove the artifactual moment for each experimental configuration. For this purpose, two assumptions were made. The first assumption was that there was no joint resisting moment at 0º of flexion, and hence that the measured resisting moment was due to imprecise positioning of the specimen. The second assumption was that the artifactual moment varied linearly with respect to flexion. Using these two assumptions a y-intercept could be determined, as well as a slope. In formulating this equation, the y-intercept was set equal to the negative of the peak moment observed between 0 and 5º of flexion. The slope of the artifact-

removal equation was set equal to the negative of the "½ Posterior Capsule Detachment" trial slope (black curve slope in Figure 59), as it exhibited the highest linearity of all experimental configurations. The corrected resisting moments are illustrated in Figure 60.
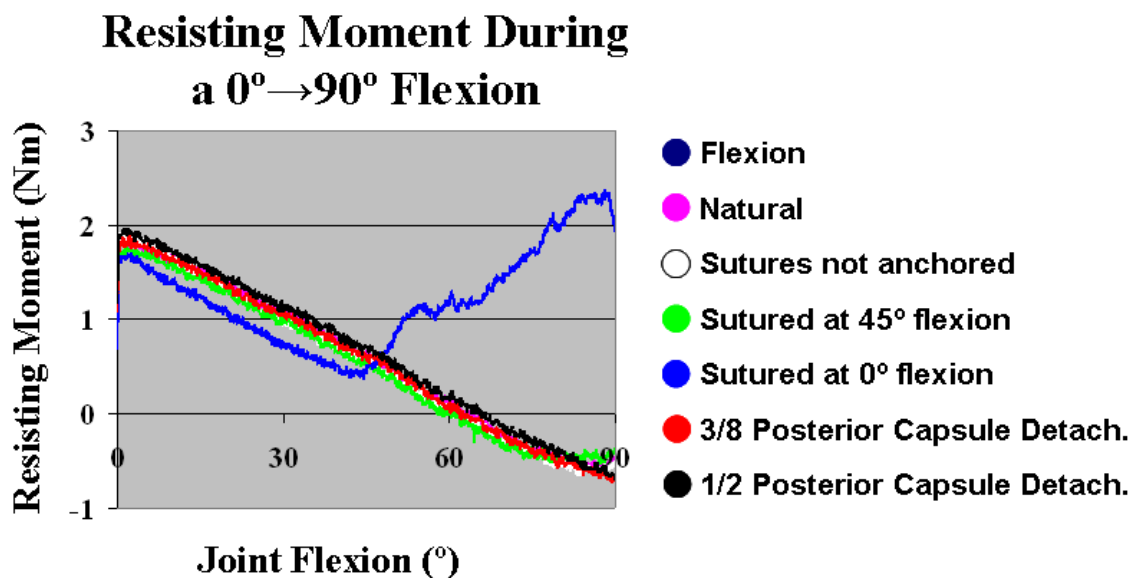


Figure 59. Plot of joint flexion versus resisting moment. A clear linear relationship is observed between the resisting moment and joint flexion.

In regards to the primary research aim, which was to provide data that could be used to provide cadaveric validation to the current hip capsule FE model, the above-described flexion test fully succeeded. Not only was it shown that tight posterior

## Resisting Moment During a 0°→90° Flexion
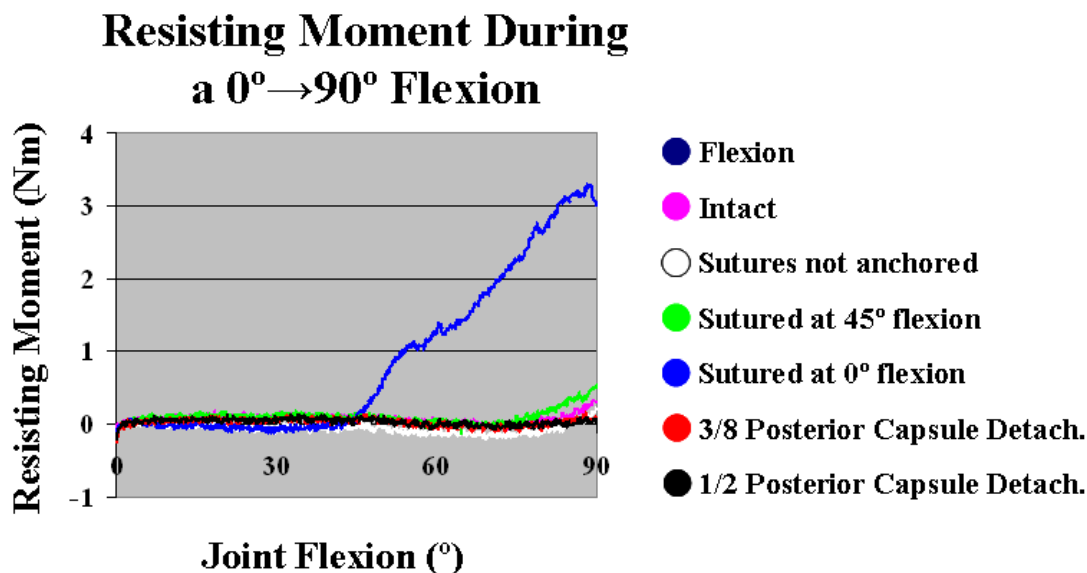


Figure 60. Graph of the resisting moments after the artifactual moment had been compensated.

capsule attachment could greatly increase the resisting moment incurred during flexion for the joint, but it was also shown that this was not a realistic modeling condition for native hips. The FE hip capsule model was subsequently modified to reflect this behavior, as opposed to that model's earlier implementation of tight attachment positioning in the capsule.

### 5.2 Sit-to-Stand Testing of Cadaveric Specimens with THA Hardware

The sit-to-stand experiment demonstrated the full capabilities of the hip simulator, and represented a type of experiment that the device had been designed to execute. In the sit-to-stand experiment, a cadaveric specimen with surgically placed implant components and intact capsule was used to simulate a clinically relevant kinematic challenge that frequently results in dislocation. The JC of the specimen was accurately determined, and the specimen was positioned within the machine so that the JC and hip simulator COR were aligned with an accuracy exceeding design targets. This is indicated by the small

nominal moments measured during axial loading (< 1Nm). During axial loading, the moments would be expected to be proportional to the placement error of the specimen and the axial load. Thus, a low moment with a 300N axial load indicates that the JC of the specimen was well aligned with the COR of the hip simulator. The forces and moments that were measured during the kinematic challenge were processed, and provided data in a format that allowed comparisons to be made between testing conditions. Impingement events could be identified, and hip capsule contribution to resisting moment magnitude could be determined.

The outcome of the sit-to-stand experiment represented a complete system test. It demonstrated success of the specimen preparation procedure, of the joint center determination protocol and post-processor algorithm, and of overall functionality of the hip simulator. Clearly, the upgraded hip simulator met its design goals, proving itself to be a sophisticated testing device.

### 5.2.1 Placement Accuracy of the Poly Liners

The placement accuracy of the poly liners (see Table 1, page 63) was dependent upon the experienced orthopaedic surgeon performing the transpelvic implantation procedure. X-rays were taken of the specimen once the procedure had concluded, but a single coronal view was insufficient for determining the orientation of the poly liners. In order to evaluate the orientation of the poly liners, cup anteversion, cup tilt, and impingement-free ROM (quantified by flexion) were compared to a set FE results. In the FE model, the impingement-free ROM (quantified by flexion) for a range of cups with varying anteversions and tilts were evaluated. The FE model used kinematics similar to those used in the sit-to-stand challenge. The results, comprised of an impingement-free ROM specific to each cup orientation, provided a data set that could be used as metric of impingement, and of whether the poly liners used in the sit-to-stand challenge had been placed correctly.

A graph was created for each of the six cup orientations physically tested. Each graph represents a given cup anteversion. The FE-computed impingement-free ROM (for the given cup anteversion) was plotted against cup tilt. Each graph indicates how well the physically tested cup correlates with a perfectly placed cup. The error bars associated with the experimental data represent a ±5° placement error. 5° was suspected as being the precision at which an experienced orthopaedic surgeon was able to place the poly liners.
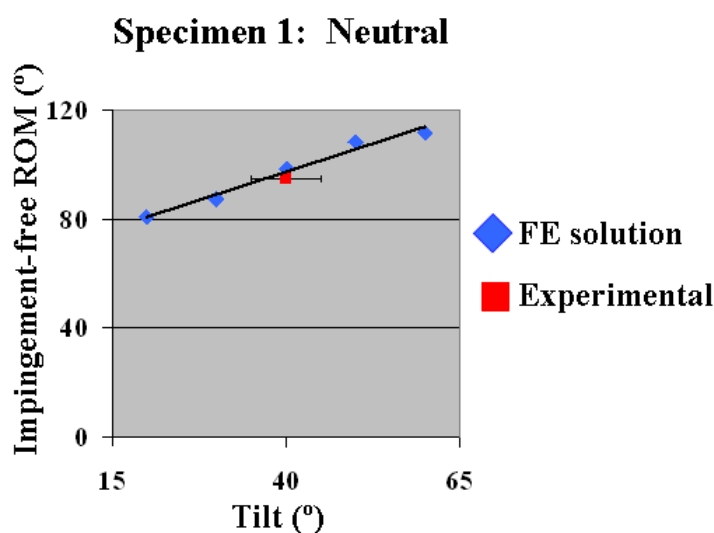


Figure 61. Graph indicating good agreement between the FE-computed solution and the experimental results, suggesting that orientation of the poly liner was correct.
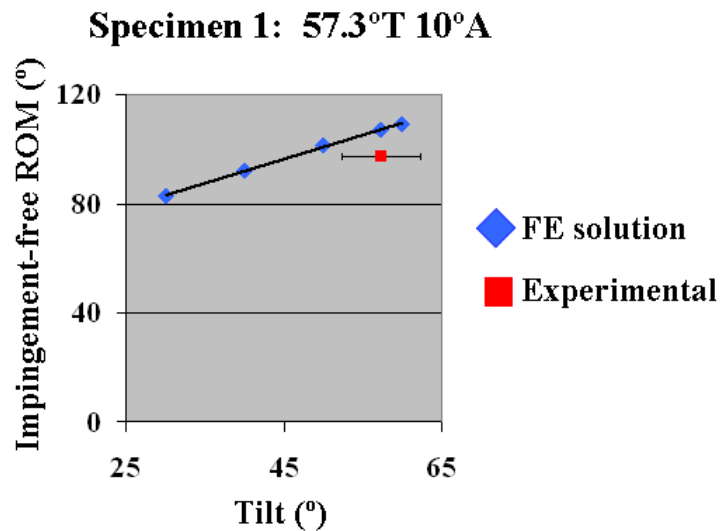
Figure 62. Graph depicting less than ideal agreement between the FE-computed solution and experimental results.
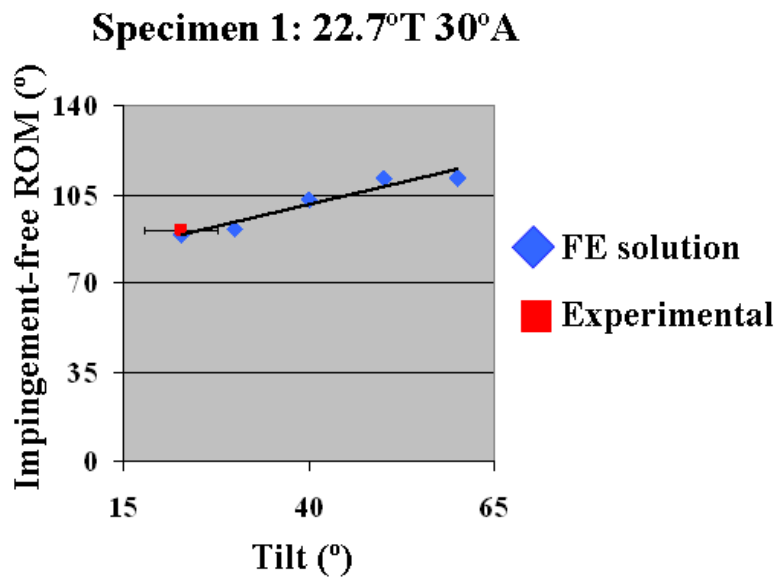


Figure 63. Graph indicating good agreement between the FE-computed solution and experimental results. The graph suggests that the orientation of the poly liner was correct.
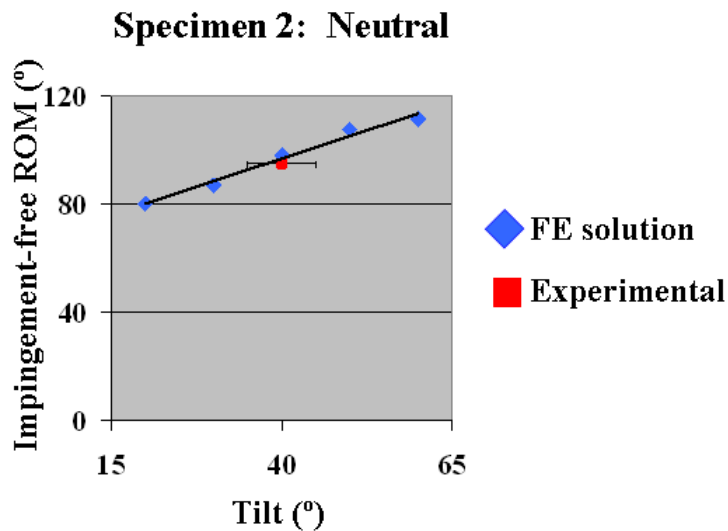
Figure 64. Graph indicating good agreement between the FE-computed solution and experimental results.
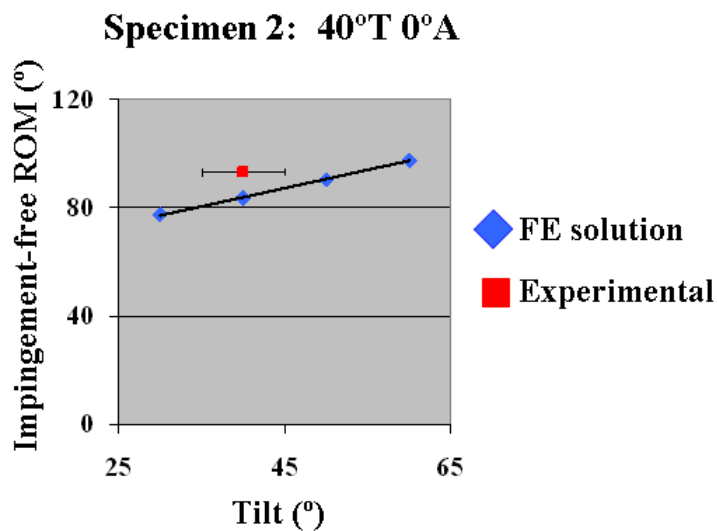


Figure 65. Graph designating less than ideal agreement between the FE-computed solution and experimental results, suggesting that the orientation of the poly liner was not 40ºT 0ºA.

## Specimen 2: 20°T 20°A
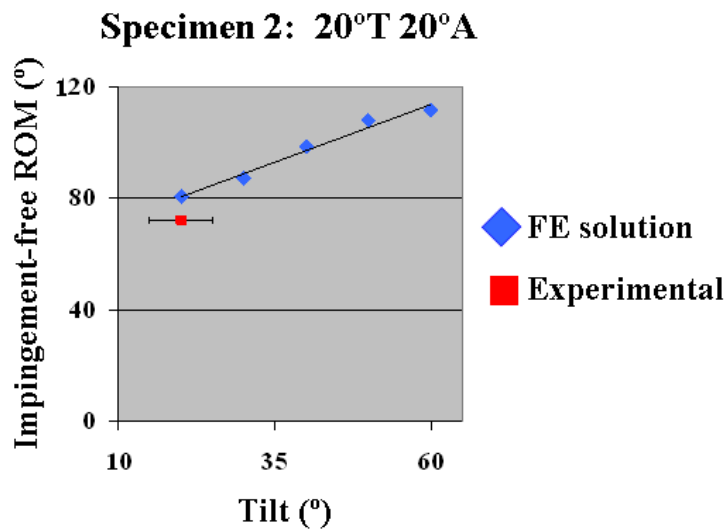


Figure 66. Graph depicting poor agreement between the FE-computed solution and experimental results, suggesting that the orientation of the poly liner was not quite 20°T 20°A.

## Specimen 3: Neutral
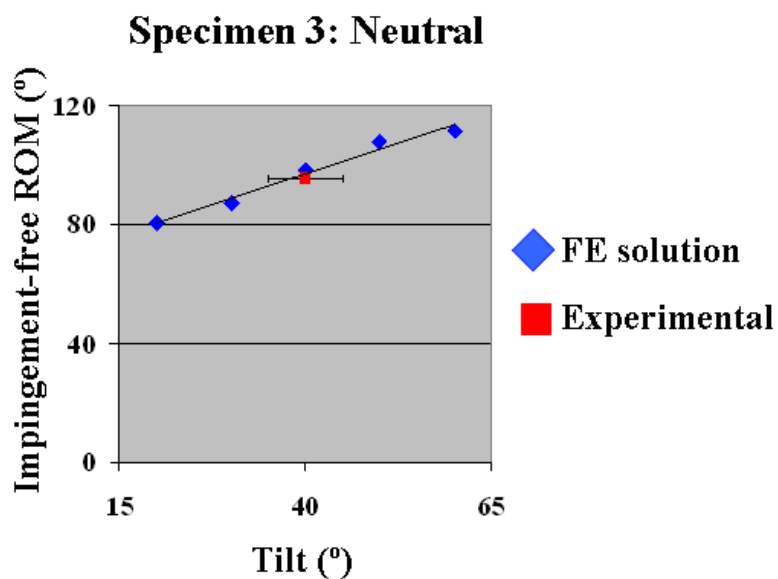


Figure 67. Graph indicating good agreement between the FE-computed solution and the experimental results, suggesting that orientation of the poly liner was correct.
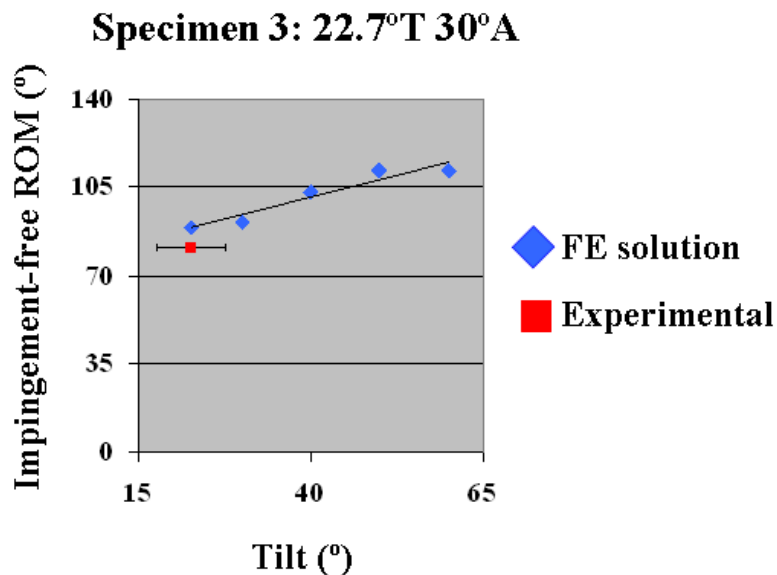
Figure 68. Graph depicting less than ideal agreement between the FE-computed solution and experimental results.

A graph of the 57.3ºT 10ºA cup of Specimen 3 was not shown as it did not impinge during testing. The graphs reveal that three of the six poly liner orientations correlated well with the FE computed solutions, suggesting that their orientations were correct. The other three poly liners appeared to have not been oriented quite correctly. This conclusion highlights an inherent issue in the transpelvic implantation procedure and cadaveric testing in general. The accuracy of the poly liner orientation is directly related to the skill of the researcher/surgeon. Given that only two specimens were tested, it was expected that with more experience, the accuracy of poly liner placement would improve. Knowing the orientation of each poly liner was important when the experimental results were compared to the FE model results. For accurate validation, both solutions needed to have equivalent setups. Without knowing the orientation of the experimental poly liner, ambiguity was introduced, and the equivalence between the FE model and experimental setup could be degraded.

To provide accurate definitions of orientations of experimentally tested poly liners, future tests should incorporate a motion capture system to spatially register the pelvis, femur, poly liner, and femoral component throughout the kinematic challenge. The use of optical motion capture for the internal hardware components (i.e. poly liner and femoral component) is possible because they have unobstructed surfaces (Figure 69).
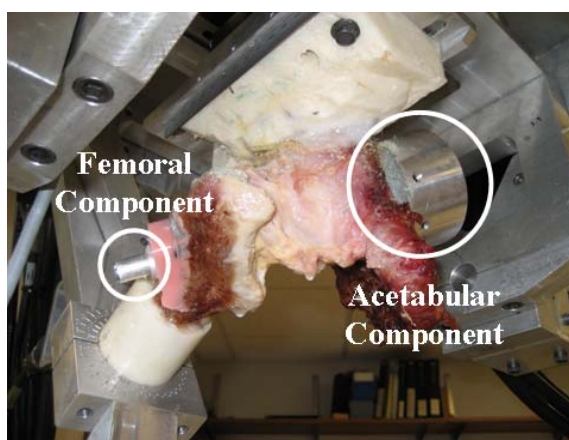


Figure 69. Photograph illustrating unobstructed surfaces of the internal hardware components.

Having such position data would improve the definitions of the poly liner orientations and specimen motion during testing, thereby reducing ambiguity with respect to poly liner orientation.

### 5.2.2 Sit-to-Stand: Specimen #1

The impingement events observed in the sit-to-stand experiment for the 22.7ºT 30ºA, Neutral, and 57.3ºT 10ºA poly liners occurred at 91º, 94.5º, and 97.5º of flexion, respectively. In an implant-only *in vitro* range of motion test reported by Burroughs et al. using the same size femoral head diameter (28mm), component-component impingement had occurred at between 99º and 117º of flexion.[33] This motion range accounts for various degrees of femoral anteversion, and neck lengths. In that paper, the acetabular

shell was positioned with 45º of tilt and 30º of anteversion. In the results reported here, the intended position of the neutral poly-liner was approximately 40º of abduction and 20º of anteversion. It would stand to reason that this low level of anteversion would lead to impingement at lesser flexion than what was observed in the Burroughs study. This corresponds well with the findings reported. The hip flexions at impingement for the three cups are just below the values reported in the Burroughs paper. The findings suggest that the poly liners in the present study were within the range of published values of surgical cup orientation.

The resisting moment curves for the neutral poly liner cases for Specimens 1 and 2 indicate that each specimen impinged at approximately the same flexion angle (94.5º and 95º, respectively). This implies that the orientations of the poly liners were consistent between specimens, and that the transpelvic implantation procedure was reproducible.

There were differences procedurally between the specimens. Specimen 1 did not benefit from coronal x-rays to check joint parameters.  These parameters include the length of the femoral neck, and distance between joint members. The accuracy with which these parameters were reproduced in a specimen determines how physiologic the capsule would behave during the kinematic challenges. It is suspected that Specimen 1 had insufficient distance between its joint members, resulting in reduced capsule tension. This impression is supported by the lack of resisting moment that was developed after 75º of flexion (see Figure 51, page 73). This angle was shown in both Specimen 2, and in the native specimen of the tight posterior capsule experiment, to be the angle of flexion at which an intact capsule began producing a resisting moment. The lack of hip capsule tension explains why the resisting moment curve of Specimen 1 (with an intact capsule) is nearly identical to that for Specimen 2 when the capsule was completely detached (see Figure 57, page 80). Not only were their peak magnitudes very close, but the curve morphologies. This indicated that the resisting moment curve of Specimen 1 was mostly due to hardware impingement rather than capsule tension. The use of coronal x-rays for

reproducing physiological joint parameters of implanted specimens is adequate for resolving this issue, and is now an integral procedural step during the transpelvic implantation procedure.

### 5.2.3 Sit-to-Stand Specimen #2

Compared to Specimen 1, Specimen 2 better reproduced physiological capsule tension. Using x-rays of the specimen taken before and after the transpelvic implantation procedure had been completed, the distance between joint members and the location of the JC could be reproduced. Evidence indicating that capsule tension was at physiologic levels was provided by the resisting moment curves of the sit-to-stand kinematic challenge. The flexion angle where a resisting moment began to develop correlated well with results attained from the intact configuration of the stiff posterior capsule attachment experiment. At approximately 75º of flexion, appreciable resisting moment developed in both experiments.

Specimen 2 was tested with an intact hip capsule, as well as with the hip capsule completely detached from the acetabulum. The resisting moment curves provided by the completely detached capsule configuration provided a better visualization of the range of motion before hardware impingement. This allowed for the effects of hardware impingement, and hip capsule to be identified and computed individually. The effects were quantified by calculating the amount of energy dissipated by the specimen during the kinematic challenge. The flexion versus resisting moment curve was integrated, providing energy in units of joules. When the energies of Specimens 1, 2, and 3 were compared for the neutral poly liner in Figure 70, the energy dissipated with the capsule intact was more than double that for an otherwise identical construct with the capsule detached. In addition to validating FE hip capsule models, the hip simulator could also be used for physically verifying FE computations for various capsule detachment

configurations. The results could be used to validate existing capsule defect and repair models.[47]

## Mechanical Energy Dissipated During Kinematic Challenge
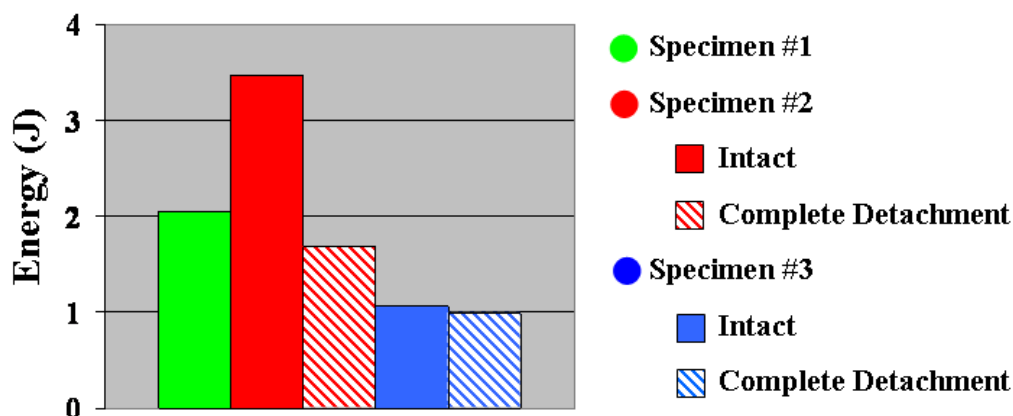


Figure 70. Graph of the mechanical energy dissipated during the sit-to-stand kinematic challenge for the intact and detached capsule configurations of Specimen 2 and Specimen 3, and the intact configuration of Specimen 1. A neutral poly liner orientation was used in all 5 instances.

### 5.2.4 Sit-to-Stand: Specimen #3

Specimen 3 was the smallest of the three specimens tested in the sit-to-stand challenge. Using the coronal x-rays of the native joints, the femoral head diameter of Specimen 3 was measured to be 44mm, while Specimens 1 and 2 were measured to be 48mm. In addition to this difference, it was also observed that Specimen 3 had a comparatively thin capsule. It is possible that these two differences account for much of the differences between peak resisting moments among the three specimens.

The small (6%) energy difference between the intact and completely detached capsule configuration showed that the capsule did not contribute mechanically by a considerable amount during the kinematic challenge. This contrasts with Specimen 2,

where the reduction in mechanical energy was 54%, nine times that of Specimen 1, further suggesting that Specimen 3 had an abnormal capsule.

### 5.2.5 Detecting Impingement and Interpreting Data Captures

For the majority of testing configurations, the impingement event was obvious. A discontinuity in the resisting moment curve and a simultaneous discontinuity in the displacement of the femur clearly indicated impingement. However, for some testing configurations, one of these attributes something did not occur, or it occurred at different times during the kinematic challenge, making the impingement event difficult to determine. Limited information was available for understanding the cause of discontinuities in the resisting moment curves that did not coincide with femur translation. Whether the moment discontinuities may have been due to soft tissue impingement, soft tissue rupture, tightening of capsular ligaments, hardware-impingement, or hardware-tissue interactions, the data captures provide little direct evidence indicating the cause.

This uncertainty provides a significant focus for future methodological improvements. Initial steps to improving data analysis techniques might be to record spatial information of the pelvis, femur, poly liner, and femoral component during experiments using an optical motion capture system. Not only would component orientation be then known, but the exact instant of impingement, the magnitudes of subluxation, and occurrence of dislocation could all be readily calculated from the resulting data. Moreover, the spatial data of the poly liner and femoral component could be used to indicate locations of the impingement and egress sites. This detailed information could be used in further validating the FE model.

A few logistical issues remain that prevent the implementation of recording spatial information. The acetabular and femoral hardware components would have to be

modified to support optical markers. The inside of the hip simulator would have to be void of all reflectance, to avoid false marker readings. This would require significant effort, to either coat the surfaces, or to have the hip simulator anodized in order to remove any reflective surfaces. More time consuming is the effort that would be required to create analysis software that could provide meaningful data (i.e. quantified subluxation) and visually represent the experimental setup, given the optical motion capture data. Despite these hurdles, the added value of position data for the implant components and specimen is almost too appealing to forego. This additional information would resolve a number of limitations, both methodological (inconsistent poly liner orientation) and fundamental (intact capsule prevents visual confirmation of impingement).

## 5.3 Conclusion

The contribution this research provides to the study of dislocation and its prevention is best viewed as a cooperative effort with the FE analysis. The hip simulator is a sophisticated device able to physically test cadaver hips and to quantify realistic dislocation events, while capturing relevant joint forces and resisting moments. A variety of clinically significant parameters can be tested: prosthesis geometry and prosthesis placement, mechanical contribution of soft tissue, joint kinematics, and joint loading. The simulator fills a large void in current dislocation research. In objectively combining supposed risk factors for dislocation, and observing dislocation with respect to a number of such factors, the hip simulator represents a significant improvement over retrospective observational studies and single-parameter *in vitro* experiments. However, cadaveric physical testing cannot be viewed as a panacea for dislocation research. A number of parameters important to dislocation cannot be fully controlled. Tissue quality and material properties, size, shape, and precise prosthesis placement are factors that need to be considered. Cadaveric testing is only part of the answer for dislocation research. The use of a physically validated FE model to study dislocation is complimentary to cadaveric

*in vitro* testing. FE analysis provides the means to test almost limitless combinations of variables pertaining to dislocation. In this respect, the main success of the hip simulator is as a validation tool for a novel FE hip capsule model. The results of both the physical sit-to-stand kinematic challenge and computational equivalent are provided in Figure 71.
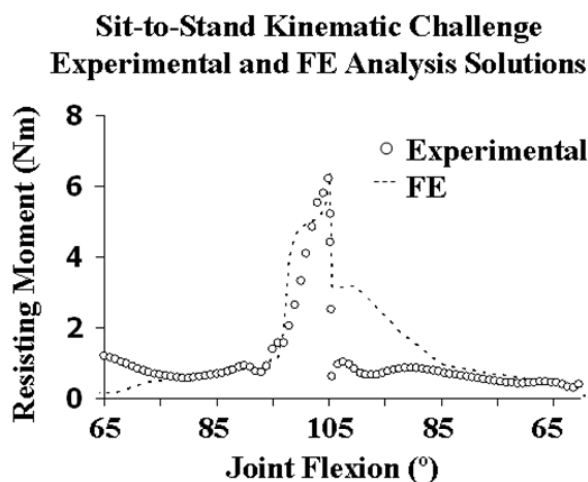


Figure 71. Plot of corresponding experimental and FE analysis solutions for the sit-to-stand challenge.

The successful completion of the experiments presented in this research achieved the research aims presented in Chapter 1. In all but one instance, the specimen was placed within the hip simulator with an appropriate joint center. The specimen preparation procedure proved successful, as it was used to prepare three specimens with equivalent orientations with respect to their PMMA bases. The hip simulator was successfully used for simulating clinically relevant dislocation-prone joint motions. Joint forces and moments were subsequently determined, allowing for comparisons to be made between specimens. Most importantly, the results of the cadaveric experiments provided validation for the FE model. In doing so, more complex kinematic challenges can be explored, and a near limitless combination of parameters and their role in dislocation may be considered.

# REFERENCES

1. Burns AWR, Bourne RB. Economics of revision total hip arthroplasty. Current Orthopaedics 2006;20(3):203-7.

2. Chang RW, Pellissier JM, Hazen GB. A cost-effectiveness analysis of total hip arthroplasty for osteoarthritis of the hip. Jama-Journal of the American Medical Association 1996;275(11):858-65.

3. Ulrich SD, Seyler TM, Bennett D, Delanois RE, Saleh KJ, Thongtrangan I, Kuskowski M, Cheng EY, Sharkey PF, Parvizi J, Stiehl JB, Mont MA. Total hip arthroplasties: What are the reasons for revision? Int Orthop 2008;32(5):597-604.

4. Ethgen O, Bruyere O, Richy F, Dardennes C, Reginster JY. Health-related quality of life in total hip and total knee arthroplasty - A qualitative and systematic review of the literature. Journal of Bone and Joint Surgery-American Volume 2004;86A(5):963-74.

5. Berry DJ, Harmsen WS, Cabanela ME, Morrey BF. Twenty-five-year survivorship of two thousand consecutive primary charnley total hip replacements - factors affecting survivorship of acetabular and femoral components. Journal of Bone and Joint Surgery-American Volume 2002 FEB;84A(2):171-7.

6. Eisler T, Svensson O, Tengstrom A, Elmstedt E. Patient expectation and satisfaction in revision total hip arthroplasty. J Arthroplasty 2002;17(4):457-62.

7. Older J. Charnley low-friction arthroplasty - A worldwide retrospective review at 15 to 20. J Arthroplasty 2002;17(6):675-80.

8. Furnes O, Lie SA, Espehaug B, Vollset SE, Engesaeter LB, Havelin LI. Hip disease and the prognosis of total hip replacements - A review of 53 698 primary total hip replacements reported to the norwegian arthroplasty register 1987-99. Journal of Bone and Joint Surgery-British Volume 2001;83B(4):579-86.

9. Ramiah RD, Ashmore AM, Whitley E, Bannister GC. Ten-year life expectancy after primary total hip replacement. The Journal of Bone & Joint Surgery 2007;89-B(10):1299.

10. Lie SA, Havelin LI, Furnes O, Engesaeter LB, Vollset SE. Failure rates for 4762 revision total hip arthroplasties in the norwegian arthroplasty register. The Journal of Bone & Joint Surgery 2004;86-B:504.

11. Lubbeke A, Moons KGM, Garavaglia G, Hoffmeyer P. Outcomes of obese and nonobese patients undergoing revision total hip arthroplasty. Arthritis & Rheumatism-Arthritis Care & Research 2008;59(5):738-45.

12. Iorio R, Healy WL, Richards JA. Comparison of the hospital cost of primary and revision total hip arthroplasty after cost containment. Orthopedics 1999;22(2):185-9.

13. Bozic KJ, Durbhakula S, Berry DJ, Naessens JM, Rappaport K, Cisternas M, Saleh KJ, Rubash HE. Differences in patient and procedure characteristics and hospital resource use in primary and revision total joint arthroplasty - A multicenter study. J Arthroplasty 2005;20(7):17-25.

14. Kurtz SM, Ong KL, Schmier J, Mowat F, Saleh K, Dybvik E, Karrholm J, Garellick G, Havelin LI, Furnes O, Malchau H, Lau E. Future clinical and economic impact of revision total hip and knee arthroplasty. Journal of Bone and Joint Surgery-American Volume 2007;89A:144-51.

15. Bozic KJ, Kurtz SM, Lau E, Ong K, Vail TP, Berry DJ. The epidemiology of revision total hip arthroplasty in the united states. Journal of Bone and Joint Surgery-American Volume 2009 JAN;91A(1):128-33.

16. Soong M, Rubash HE, Macaulay W. Dislocation after total hip arthroplasty. J Am Acad Orthop Surg 2004;12(5):314-21.

17. Palan J, Beard DJ, Murray DW, Andrew JG, Nolan J. Which approach for total hip arthroplasty: Anterolateral or posterior? Clin Orthop 2009;467(2):473-7.

18. Gibson A. Posterior exposure of the hip joint. The Journal of Bone & Joint Surgery 1950;32-B(2).

19. Hoppenfeld S, deBoer P, Buckley R. Surgical exposures in orthopaedics: The anatomic approach. 3rd ed. Philadelphia, PA: Wolters Kluwer/Lippincott Williams and Wilkins; 2003. .

20. Muller ME. Total hip prostheses. Clin Orthop 1970(72):46,&.

21. Masonis JL, Bourne RB. Surgical approach, abductor function, and total hip arthroplasty dislocation. Clin Orthop 2002(405):46-53.

22. Witzleb WC, Stephan L, Krummenauer F, Neuke A, Gunther KP. Short-term outcome after posterior versus lateral surgical approach for total hip arthroplasty - a randomized clinical trial. Eur J Med Res 2009;14(6):256-63.

23. Brown TD, Callaghan JJ. Impingement in total hip replacement: Mechanisms and consequences. Current Orthopaedics 2008;22(6):376-91.

24. Kwon MS, Kuskowski M, Mulhall KJ, Macaulay W, Brown TE, Saleh KJ. Does surgical approach affect total hip arthroplasty dislocation rates? Clin Orthop 2006(447):34-8.

25. Chivas AJ, Smith K, Tanzer M. Role of capsular repair on dislocation in revision total hip arthroplasty. Clin Orthop 2006(453):147-52.

26. Tsai SJ, Wang CT, Jiang CC. The effect of posterior capsule repair upon post-operative hip dislocation following primary total hip arthroplasty. Bmc Musculoskeletal Disorders 2008;9.

27. Pellicci PM, Bostrom M, Poss R. Posterior approach to total hip replacement using enhanced posterior soft tissue repair. Clin Orthop 1998(355):224-8.

28. Kim YS, Kwon SY, Sun DH, Han SK, Maloney WJ. Modified posterior approach total to hip arthroplasty to enhance joint stability. Clin Orthop 2008;466(2):294-9.

29. White RE, Forness TJ, Allman JK, Junick DW. Effect of posterior capsular repair on early dislocation in primary total hip replacement. Clin Orthop 2001(393):163-7.

30. Weeden SH, Paprosky WG, Bowling JW. The early dislocation rate in primary total hip arthroplasty following the posterior approach with posterior soft-tissue repair. J Arthroplasty 2003;18(6):709-13.

31. Stahelin T, Vienne P, Hersche O. Failure of reinserted short external rotator muscles after total hip arthroplasty. J Arthroplasty 2002;17(5):604-7.

32. Stahelin T, Drittenbass L, Hersche O, Miehlke W, Munzinger U. Failure of capsular enhanced short external rotator repair after total hip replacement. Clin Orthop 2004(420):199-204.

33. Burroughs BR, Hallstrom B, Golladay GJ, Hoeffel D, Harris WH. Range of motion and stability in total hip arthroplasty with 28-, 32-, 38-, and 44-mm femoral head sizes - an in vitro study. J Arthroplasty 2005;20(1):11-9.

34. Noble LD, Colbrunn RW, Lee DG, van den Bogert AJ, Davis BL. Design and validation of a general purpose robotic testing system for musculoskeletal applications. Journal of Biomechanical Engineering-Transactions of the Asme 2010;132(2).

35. Peters CL, McPherson E, Jackson JD, Erickson JA. Reduction in early dislocation rate with large-diameter femoral heads in primary total hip arthroplasty. J Arthroplasty 2007;22(6):140-4.

36. Hummel MT, Malkani AL, Yakkanti MR, Baker DL. Decreased dislocation after revision total hip arthroplasty using larger femoral head size and posterior capsular repair. J Arthroplasty 2009;24(6):73-6.

37. Amstutz HC, Le Duff MJ, Beaule PE. Prevention and treatment of dislocation after total hip replacement using large diameter balls. Clin Orthop 2004(429):108-16.

38. Lewinnek GE, Lewis JL, Tarr R, Compere CL, Zimmerman JR. Dislocations after total hip-replacement arthroplasties. Journal of Bone and Joint Surgery-American Volume 1978;60(2):217-20.

39. Pedersen DR, Callaghan JJ, Brown TD. Activity-dependence of the "safe zone" for impingement versus dislocation avoidance. Medical Engineering & Physics 2005;27:323.

40. Nishii T, Sugano N, Miki H, Koyama T, Takao M, Yoshikawa H. Influence of component positions on dislocation - computed tomographic evaluations in a consecutive series of total hip arthroplasty. J Arthroplasty 2004;19(2):162-6.

41. Mccollum DE, Gray WJ. Dislocation after total hip-arthroplasty - causes and prevention. Clin Orthop 1990(261):159-70.

42. Ali Khan MA, Brakenbury PH, Reynolds IS. Dislocation following total hip replacement. J Bone Joint Surg Br 1981;63-B(2):214-8.

43. Biedermann R, Tonin A, Krismer M, Rachbauer F, Eibl G, Stockl B. Reducing the risk of dislocation after total hip arthroplasty - the effect of orientation of the acetabular component. Journal of Bone and Joint Surgery-British Volume 2005;87B(6):762-9.

44. Rittmeister M, Callitsis C. Factors influencing cup orientation in 500 consecutive total hip replacements. Clin Orthop Relat Res 2006;445:192-6.

45. Paterno SA, Lachiewicz PF, Kelley SS. The influence of patient-related factors and the position of the acetabular component on the rate of dislocation after total hip replacement. Journal of Bone and Joint Surgery-American Volume 1997;79A(8):1202-10.

46. Alberton GM, High WA, Morrey BF. Dislocationm after revision total hip arthroplasty - an analysis of risk factors and treatment options. Journal of Bone and Joint Surgery-American Volume 2002;84A(10):1788-92.

47. Elkins JM, Stroud NJ, Rudert MJ, Tochigi YT, Pedersen DR, Ellis BJ, Callaghan MD, Weiss JA, Brown TD. The capsule's contribution to total hip construct stability-a finite element analysis. Clin Orthop Relat Res 2010;Submitted.

48. Elkins JM, Ryan P, Tochigi Y, Pedersen DR, Ellis BJ, Callaghan JJ, Weiss JA, Brown TD. The capsule's contribution to total hip construct stability- a finite element analysis. Hip Society Award Submission 2009.

49. Agur AMR, Dalley AF. Grant's atlas of anatomy. 11th ed. Philadelphia, PA: Lippincott William & Wilkins; 2005. .

50. Affatato S, Spinelli A, Zavalloni M, Mazzega-Fabbro C, Viceconti A. Tribology and total hip joint replacement: Current concepts in mechanical simulation. Med Eng Phys 2008;30(10):1305-17.

51. Kiguchi K, Horie T, Yamashita A, Ueno M, Kobayashi T, Mawatari M, Hotokebuchi T. A study of the effect of the femoral head diameter on prosthetic hip joint dislocation using a hip-joint motion simulator. Conf Proc IEEE Eng Med Biol Soc 2009;1:6058-61.

52. Bader R, Scholz R, Steinhauser E, Zimmermann S, Busch R, Mittelmeier W. The influence of head and neck geometry on stability of total hip replacement - A mechanical test study. Acta Orthop Scand 2004;75(4):415-21.

53. Bottros JJ, Greeson CB, Colbrunn RW, van den Bogert AJ, Barsoum WK. Evaluation of the acetabular labrum in impingement free range of motion and dislocation using a novel cadaveric robotics model. 2010.

54. Heiner AD, Lundberg HJ, Baer TE, Pedersen DR, Callaghan JJ, Brown TD. Effects of episodic subluxation events on third body ingress and embedment in the THA bearing surface. J Biomech 2008;41(10):2090-6.

55. Cristofolini L, Varini E, Viceconti M. In-vitro method for assessing femoral implant-bone micromotions in resurfacing hip implants under different loading conditions. Proceedings of the Institution of Mechanical Engineers Part H-Journal of Engineering in Medicine 2007;221(H8):943-50.

56. Anderson AE, Ellis BJ, Maas SA. Validation of finite element predictions of cartilage contact pressure in the human hip joint. Journal of Biomechanical Engineering 2008;130:051008-1.

57. Meneghini RM, Hallab NJ, Berger RA, Jacobs JJ, Paprosky WG, Rosenberg AG. Stem diameter and rotational stability in revision total hip arthroplasty: A biomechanical analysis. J Orthop Surg Res 2006;1:5.

58. Bishop NE, Waldow F, Morlock MM. Friction moments of large metal-on-metal hip joint bearings and other modern designs. Med Eng Phys 2008;30(8):1057-64.

59. Stagni R, Leardini A, Cappozzo A, Benedetti MG, Cappello A. Effects of hip joint centre mislocation on gait analysis results. J Biomech 2000 NOV;33(11):1479-87.

60. Ehrig RM, Taylor WR, Duda GN, Heller MO. A survey of formal methods for determining the centre of rotation of ball joints. J Biomech 2006;39:2798-809.

61. Camomilla V, Cereatti A, Vannozzi G, Cappozzo A. An optimized protocol for hip joint centre determination using the functional method. J Biomech 2006;39(6):1096-106.

62. Cappozzo A, Catani F, Della Croce U, Leardini A. Position and orientation in-space of bones during movement - anatomical frame definition and determination. Clin Biomech 1995;10:171-8.

63. Gamage SSHU, Lasenby J. New least squares solutions for estimating the average centre of rotation and the axis of rotation. J Biomech 2002;35(1):87-93.

64. Chernov N, Camomilla V, Cappozzo A. Estimation of the centre of rotation: A methodological contribution. Journal of Biomechanics 2004;37:413.

65. Pratt VR. Direct least-squares fiting of algebraic surfaces. Computer Graphics;21:145.

66. Shabana AA. Computational dynamics. Second ed. New York, NY: John Wiley & Sons, Inc; 2001. .

67. Schrand D. Crosstalk compensation using matrix methods. Network System Designline 2007.

68. Piazza SJ, Okita N, Cavanagh PR. Accuracy of the functional method of hip joint center location: Effects of limited motion and varied implementation. J Biomech 2001;34(7):967-73.

69. Leardini A, Cappozzo A, Catani F, Toksvig-Larsen S, Petitto A, Sforza VC, G., Giannini S. Validation of a functional methodf or the estimation of hip joint centre location. J.Biomech. 1999;32(1).

70. Johnson RC, Brand RA, Crowninshield RD. Reconstruction of the hip. A mathmatical approach to determine optimum geometric relationships. The Journal of Bone & Joint Surgery 1979;61(5):639.

71. Piazza SJ, Erdemir A, Okita N, Cavanagh PR. Assessment of the functional method of hip joint center location subject to reduced range of hip motion. J Biomech 2004;37(3):349-56.